# Phase-separating fusion proteins drive cancer by dysregulating transcription through ectopic condensates

Nazanin Farahi [1,2,#], Tamas Lazar [1,2,#], Peter Tompa [1,2,3], Bálint Mészáros [4,5]*, Rita Pancsa [3,]*

[1] VIB-VUB Center for Structural Biology, Vlaams Instituut voor Biotechnologie (VIB), Pleinlaan 2, 1050 Brussels, Belgium
[2] Structural Biology Brussels, Vrije Universiteit Brussel (VUB), Pleinlaan 2, 1050 Brussels, Belgium
[3] Institute of Enzymology, HUN-REN Research Centre for Natural Sciences, 1117 Budapest, Hungary
[4] Structural and Computational Biology Unit, European Molecular Biology Laboratory (EMBL), 69117 Heidelberg, Germany
[5] St Jude Children's Research Hospital, 262 Danny Thomas Place, 38105 Memphis, TN, USA

[#] co-first authors
* corresponding authors
Correspondence may be addressed to: Rita Pancsa (pancsa.rita@ttk.hu) or Bálint Mészáros (balint.meszaros@stjude.org)

# Abstract

Numerous cellular processes rely on biomolecular condensates formed through liquid-liquid phase separation (LLPS), thus, perturbations of LLPS underlie various diseases. We found that proteins initiating LLPS are frequently implicated in somatic cancers, even surpassing their involvement in neurodegeneration. Cancer-associated LLPS scaffolds are connected to all cancer hallmarks and tend to be oncogenes with dominant genetic effects lacking therapeutic options. Since most of them act as oncogenic fusion proteins (OFPs), we undertook a systematic analysis of cancer driver OFPs by assessing their module-level molecular functions. We identified both known and novel combinations of molecular functions that are specific to OFPs and thus have a high potential for driving tumorigenesis. Protein regions driving condensate formation show an increased association with DNA- or chromatin-binding domains of transcription regulators within OFPs, indicating a common molecular mechanism underlying several soft tissue sarcomas and hematologic malignancies where phase-separation-prone OFPs form abnormal, ectopic condensates along the DNA, and thereby dysregulate gene expression programs.

**Keywords**: liquid-liquid phase separation, biomolecular condensates, membraneless organelles, cancer, somatic mutations, gene fusion, oncogenic fusion proteins

# Introduction

Many proteins and nucleic acids are able to undergo liquid-liquid phase separation (LLPS) and form biomolecular condensates in living cells[1]. These condensates, also frequently referred to as membraneless organelles (MLOs), are non-stoichiometric assemblies of macromolecules comprising a distinct liquid-like phase[2] dedicated to specific cellular functions[3,4]. In the last few years, LLPS has emerged as a general and fundamental organizing principle employed by both prokaryotic and eukaryotic cells for the spatiotemporal segregation of their metabolic and signaling processes[5,6].

Proteins play distinct roles in LLPS, classified as *scaffolds* (also termed as *LLPS drivers* but here we will reserve this word for cancer drivers), regulators and clients. *Scaffolds* can phase-separate on their own or in combination with other scaffolds (proteins, DNA or RNA), under native-like conditions. Regulators influence LLPS through affecting the expression, localization or modification states of the scaffolds. C*lients* do not influence LLPS but enter the condensates and may contribute to their functions[3,7].

Although LLPS processes show a great heterogeneity in terms of the participating macromolecules and underlying molecular driving forces, they uniformly rely on multivalent weak/transient interactions between the (co)scaffolds that provide the flexibility required for the dynamic rearrangements crucial for LLPS[1]. Intrinsically disordered regions (IDRs), often of low sequence complexity, can play key roles in LLPS, usually by mediating weak residue-residue interactions[8–10], or by carrying short linear motifs (SLiMs[11]) that bind to folded domains[12,13]. Homo-oligomerization is also frequently exploited by LLPS scaffolds to increase their valences[3,10,14], and the binding of nucleic acids through RNA- or DNA-binding domains, or IDRs is also typical[15,16]. Elucidating the mechanism of formation, functions and regulation of LLPS systems remains a challenging task[17]. Nonetheless, many such systems have already been described, and several dedicated LLPS databases became available[5,18–20] providing rich annotations enabling potential generalizations on the associated proteins[21].

Numerous crucial cellular processes rely on phase-separated condensates, for instance, transcription and its regulation rely on RNA polymerase II condensates[22], super enhancers[23] and chromatin compartments with distinct histone modification patterns[24,25]. Therefore, perturbations of LLPS and the associated condensates can readily lead to the development of various diseases[26,27]. Phase-separated liquid-like structures can make a transition into less dynamic hydrogels or amyloid-like protein aggregates that are associated with certain neurodegenerative diseases[28,29], such as amyotrophic lateral sclerosis[30,31] and Alzheimer's disease[32]. RNA-binding proteins are abundantly represented among LLPS scaffolds[10] and are implicated in diverse diseases, such as neurodegenerative disorders, muscular atrophies and cancer[33].

The development of somatic cancers was generally attributed to the accumulation of driver mutations that alter the stability, activity or interactions of key proteins. However, recently it became evident that mutations can also interfere with and/or over-activate the formation of phase-separated condensates[34]. The presence or absence of certain MLOs are accepted diagnostic markers of certain cancer types[34]. For example, enlarged nucleoli are characteristic of large-cell lung carcinoma, or the lack of promyelocytic leukemia (PML) bodies are distinctive of acute promyelocytic leukemia[34]. Cancer-associated mutations directly affecting LLPS have only been demonstrated for some proteins[35–40]. Large-scale computational analyses highlighted that proteins implicated in diseases, including cancer, are

81 enriched in predicted LLPS propensity[41]. Also, thousands of disease mutations have been identified in
82 predicted LLPS scaffolds that likely contribute to condensate dysregulation[42].
83 The role of LLPS in cancer has been extensively investigated and reviewed recently[25,43–49]. In two
84 recent studies, cancer was linked with LLPS of the products of oncogenic fusions resulting from
85 chromosomal rearrangements. In one, experimental and computational analysis of a large number of
86 cancer-related fusion proteins have shown their propensity to be localized in cellular condensates[50]. In
87 the other[51], LLPS of a few fusion proteins combining phase-separating and DNA-binding regions have been
88 experimentally confirmed. More interestingly, they have been shown to be targetable by small-molecule
89 inhibitors.
90 Here, we take a rational approach to dissect these relations. By focusing on experimentally proven
91 LLPS scaffolds and cancer drivers, we provide an unbiased assessment of the relevance of LLPS proteins
92 in cancer compared to various other disease classes. We offer a multi-level description of the biological
93 processes and functions that are preferentially associated with LLPS proteins involved in cancer and assess
94 the underlying mutational mechanisms, showing the preponderance of fusion events, especially in certain
95 early-onset somatic tumors. Using protein-region centric functional annotations, we show how they
96 combine cellular functions with the ability to drive condensation, and how these newly emerging
97 combinations of functional elements may offer novel ways of targeting this so-far largely undruggable
98 class of oncogenes.
99

# Results

## 1. LLPS scaffolds play a significant role in the development of somatic cancer

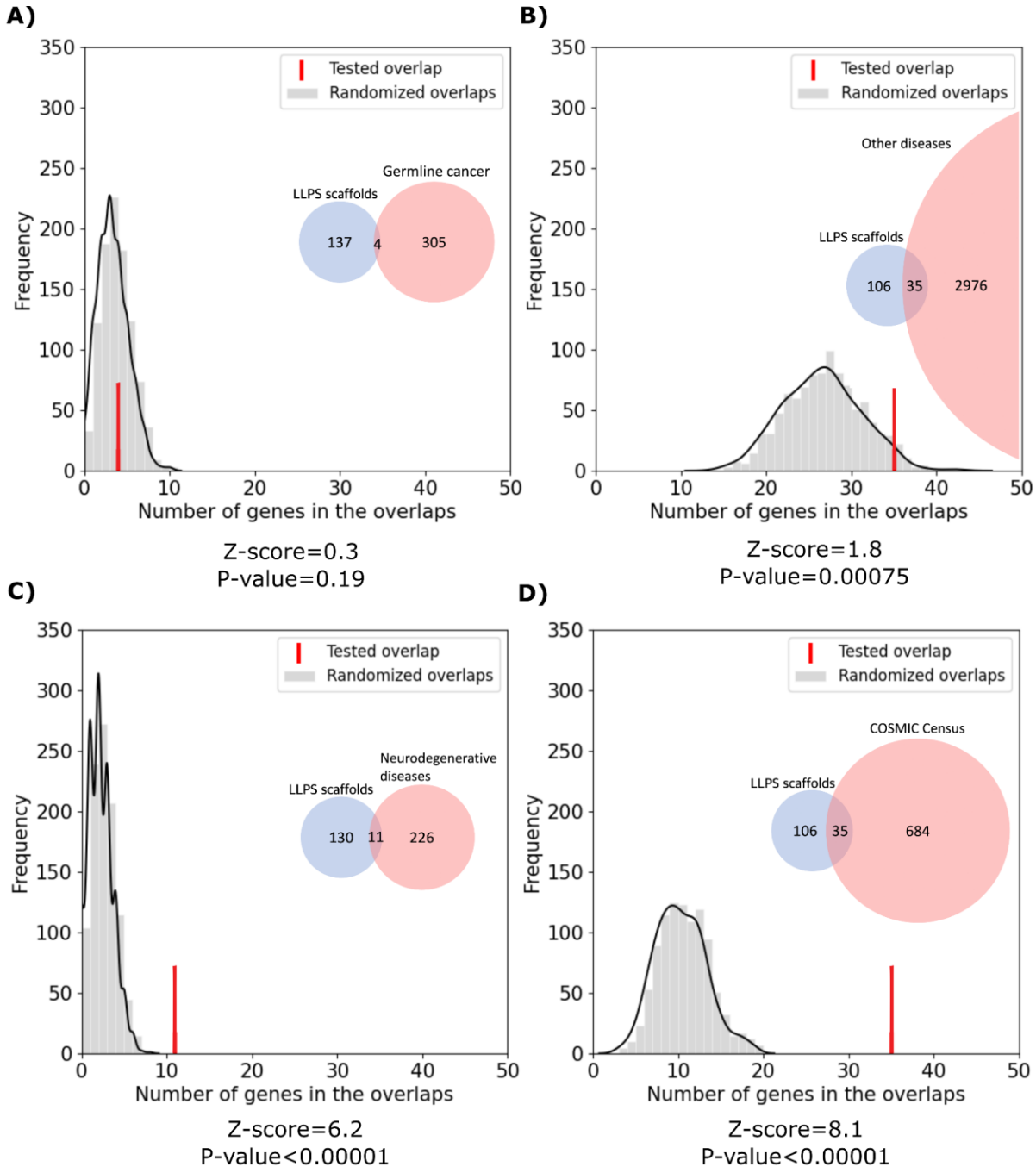


**Figure 1: Overlap between LLPS scaffolds and various disease-associated proteins.** Gray distributions show the expected overlap between LLPS scaffolds and the four classes of disease-associated proteins: (**A**) germline cancer, (**B**) other human diseases, (**C**) neurodegenerative diseases and (**D**) somatic cancer. Distributions were calculated from 1000 random generated sets of human proteins with subcellular localizations and levels of annotation matched

to the real disease protein sets (*see Data and methods*). Red bars mark the observed overlap between the true protein sets with the corresponding Z-scores and p-values indicated below the graphs. Inset Venn diagrams show the number of proteins in each set and the observed overlap between them with circle areas being proportionate to the corresponding set sizes.

In order to investigate potential links between liquid-liquid phase separation (LLPS) and proteins implicated in different groups of disease, we conducted a comprehensive analysis of the underlying associations. First, we tested how much LLPS scaffolds (**Table S1**) overlap with proteins involved in various classes of human diseases. We obtained four sets of proteins (see **Figure 1A-D** and **Table S2**) implicated in germline cancer, somatic cancer, neurodegenerative diseases and other human diseases (*see Data and methods*). For each of them, we generated 1000 random sets of human proteins with the same distributions of subcellular localizations and level of annotations (*see Data and methods and **Table S3***), and calculated the overlap with LLPS scaffolds. The distributions of overlaps between LLPS scaffolds and these random protein sets were compared to the true overlaps between LLPS scaffolds and the real disease-linked proteins of the four disease classes (**Figure 1A-D)**. Germline cancer proteins show an overlap with LLPS scaffolds that is indistinguishable from a random overlap. Other human diseases are slightly enriched in LLPS scaffolds, while neurodegenerative diseases are very significantly enriched with the observed overlap exceeding 6 standard deviations above the value expected at random. This finding conforms to previous studies elucidating the role of LLPS in neurodegenerative diseases[29,31]. However, LLPS scaffolds exhibit an even higher enrichment in somatic cancer driver genes, with the observed overlap being over 8 standard deviations higher than expected. Calculations done on a larger, but less confident dataset of LLPS scaffolds derived from PhaSepDB (**Table S4**) used as an independent alternative of our scaffold dataset also confirmed the observed tendencies (**Figure S1**). This shows that biological condensation is central to the development of somatic cancer in general. Proteins that regulate LLPS or partake in condensation in a client role only have a more moderate overlap with around 3 standard deviations above expectation level (**Figure S2**). Also, this effect is specific to condensation through LLPS, as proteins prone to aggregate through amyloid formation (**Table S5**) do not show a significant overlap with somatic cancer (**Figure S3**).

## 2. LLPS scaffolds are heavily associated with most cancer hallmarks

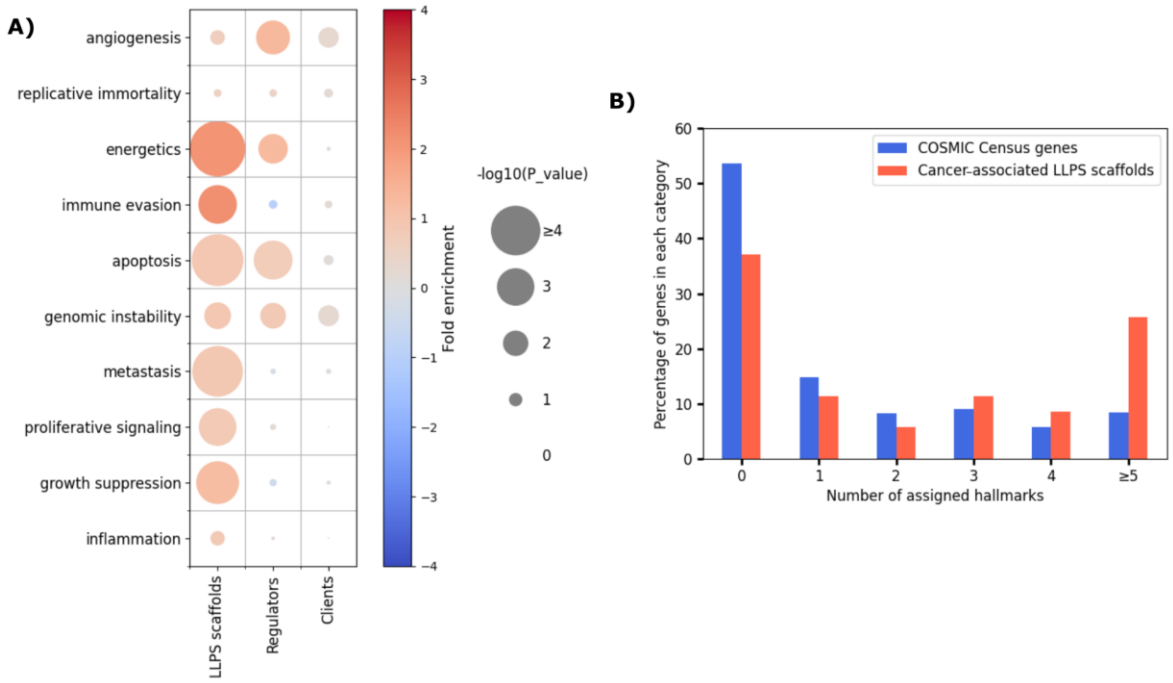


**Figure 2: Association of LLPS-related proteins with cancer hallmarks.** (**A**) The color of the circles in the heatmap represents the fold enrichment, while the size represents the significance of overrepresentation/depletion for the three classes of LLPS-related proteins in the ten hallmarks of cancer. (**B**) The histogram depicts the number of hallmarks individual cancer driving LLPS scaffolds contribute to (red) as compared to cancer drivers in general (blue).

Tumor cells are known to acquire ten common phenotypes that are referred to as the cancer hallmarks[52]. Using annotations for the known cancer drivers in COSMIC Census (**Table S6**), we analyzed how often LLPS-related cancer proteins are connected to each of these hallmarks. We focused on LLPS scaffolds, regulators and clients that are annotated as cancer drivers in COSMIC and compared their involvement in each hallmark with those of all cancer drivers (**Table S7**). **Figure 2A** shows that LLPS scaffolds are enriched in most hallmarks, with statistical significance ($p<10e-2$) in seven. PhaSepDB-derived scaffolds also confirmed this tendency (**Figure S4**). LLPS regulators also exhibit significant enrichments in four hallmarks, while LLPS clients show no significant enrichment. **Figure 2B** also shows that LLPS scaffolds more often have an effect on several hallmarks than cancer drivers in general. While hallmark annotations are obviously sparse (roughly half of all cancer drivers are not associated with any hallmark), there is a clear tendency for LLPS scaffolds influencing several hallmarks. Over 25% of cancer-driving LLPS scaffolds contribute to 5 or more hallmarks, while in general this is only true for less than 10% of all cancer drivers.

## 3. Cancer-associated LLPS proteins are enriched in critical molecular functions, including mRNA processing, transcription regulation and chromatin remodeling

To evaluate the molecular mechanisms of LLPS-related proteins in cancer, we defined 'molecular toolkits', sets of Gene Ontology terms that capture a high-level molecular function (*see **Table S8** for toolkit definitions*). We grouped our toolkits into 5 supertoolkits that cover broad, cell-level functions (**Table S9**).

164 Molecular toolkits evaluated for cancer drivers show that the most commonly affected functions are
165 heterochromatin organization, DNA binding and gene silencing, protein maturation and stability, cell
166 surface receptor signaling, intracellular signal transduction, intracellular transport, and cell adhesion
167 (**Figure 3**). Compared to cancer drivers' toolkit enrichments, LLPS scaffolds, regulators and clients all have
168 distinct toolkit repertoires (**Table S10**). Cancer driver LLPS scaffolds are most significantly linked to mRNA
169 processing, its regulation, and chromatin remodeling (see **Figure 3B** for a selection of toolkit terms that
170 show significant enrichments in LLPS-related cancer drivers). Dysregulation of LLPS regulators impacts a
171 lot more molecular processes including DNA recombination and replication, protein localization to
172 organelles, translation, regulation of gene silencing and epigenetic regulation of gene expression (**Figure**
173 **3B**). Finally, molecular functions of LLPS clients altered by cancer are most commonly associated with
174 chromosome segregation, actin and microtubule cytoskeleton organization and with regulation of
175 substrate adhesion-dependent cell spreading (**Figure 3B**).

**A**

| Supertoolkit | Toolkit name | Toolkit size (#GO terms) | Scaffolds Enriched GO terms | Regulators Enriched GO terms | Clients Enriched GO terms | Cancer Enriched GO terms |
|---|---|---|---|---|---|---|
| I. Genetic material organisation and maintenance | DNA enzymatic chemical modification | 4 | 0.00 | 0.00 | 0.00 | 0.00 |
| | DNA structural organization | 6 | 0.17 | 0.00 | 0.00 | 0.33 |
| | DNA damage repair | 2 | 0.00 | 0.00 | 0.00 | 0.00 |
| | DNA recombination | 1 | 0.00 | 1.00 | 0.00 | 0.00 |
| | DNA replication-related molecular processes | 2 | 0.00 | 1.00 | 0.50 | 0.00 |
| II. Protein availability | Transcription and gene expression regulation | 6 | 0.00 | 0.33 | 0.00 | 0.17 |
| | mRNA processing, translation and degradation | 10 | 0.50 | 0.40 | 0.10 | 0.00 |
| | Protein maturation and folding | 3 | 0.00 | 0.33 | 0.00 | 0.33 |
| | Altering and maintaining protein localization | 9 | 0.00 | 0.22 | 0.00 | 0.00 |
| | Altering protein stability and degradation | 4 | 0.00 | 0.50 | 0.00 | 0.25 |
| III. Protein activity | Modulation of macromolecular interactions | 8 | 0.00 | 0.13 | 0.00 | 0.13 |
| | Protein post-translational modification | 18 | 0.00 | 0.06 | 0.00 | 0.11 |
| | Molecular assembly and disassembly of protein complexes | 5 | 0.20 | 0.00 | 0.20 | 0.00 |
| | Regulation of catalytic activity | 1 | 0.00 | 0.00 | 0.00 | 0.00 |
| IV. Response to stimuli and flow of information | Cell surface receptor signaling | 2 | 0.00 | 0.00 | 0.00 | 0.50 |
| | Intracellular signal transduction | 1 | 0.00 | 0.00 | 0.00 | 1.00 |
| | Cytoskeletal organization | 7 | 0.00 | 0.00 | 0.43 | 0.29 |
| | Cell adhesion | 10 | 0.00 | 0.00 | 0.20 | 0.60 |
| V. Availability and flow of material | Metabolism | 13 | 0.08 | 0.00 | 0.00 | 0.00 |
| | Transport across the plasmamembrane | 5 | 0.00 | 0.00 | 0.00 | 0.20 |
| | Transport inside the cell | 5 | 0.00 | 0.20 | 0.00 | 0.20 |

**B**

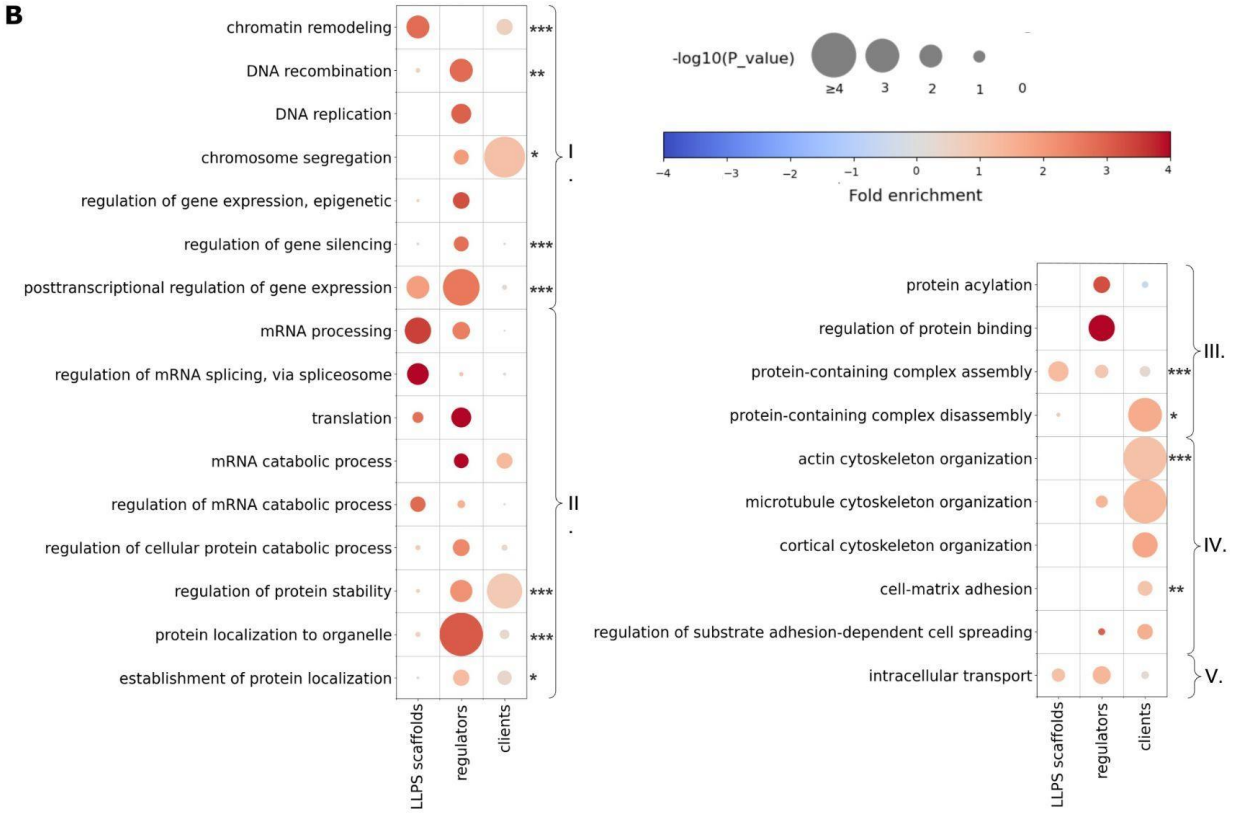


**Figure 3: Enrichment of functional toolkits in the three classes of LLPS-related proteins (scaffolds, regulators, clients).** (**A**) A particular toolkit was considered to be enriched in a protein class if the fold enrichment was ≥1 and p-value of significance was <0.05 in Fisher's exact test. (**B**) The heatmaps depict significantly enriched GO terms (fold enrichment > 1.0 by Fisher's exact test) with a minimum of 3 proteins in a given LLPS class. On the right side of the heatmap, one, two or three stars indicate the significance level of the GO enrichments for the whole set of cancer drivers compared to a random background (with levels 0.05>p≥0.01, 0.01>p≥0.001, p<0.001, respectively). GO terms

183 belonging to the same supertoolkit are connected by brackets with the numbering of supertoolkits also provided.
184 Definitions of toolkits by GO terms and their unfiltered individual fold enrichment and significance values are listed
185 in **Tables S8 and S10**.
186

187 **4. Cancer-associated LLPS scaffolds typically drive cancer via dominant gene fusions and lack**
188 **available drugs**
189

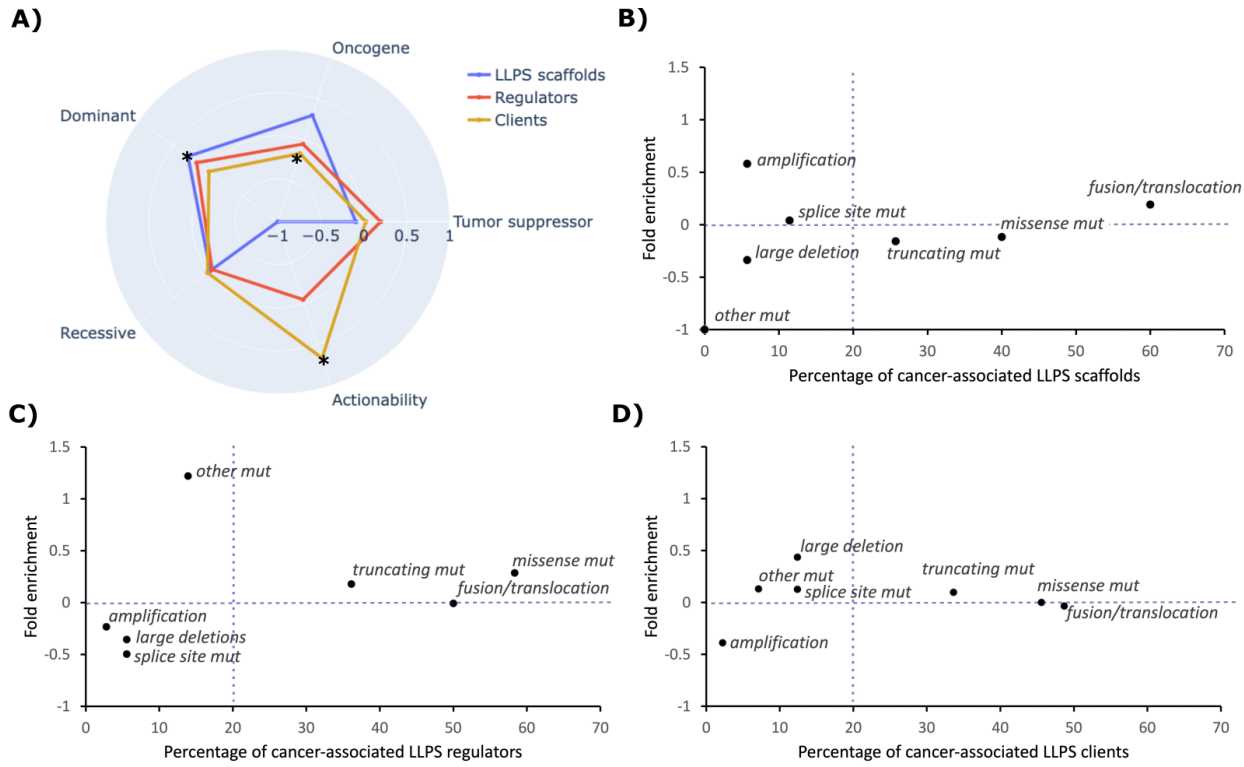

190
191

192 **Figure 4: Characteristic features of LLPS-related cancer driver proteins compared to cancer drivers in general.**
193 (**A**) The radar chart plots the fold enrichments of the three classes of cancer-associated LLPS proteins in cancer
194 drivers that are oncogenes or tumor suppressors; that are affected by dominant or recessive mutations; and those
195 with available FDA-approved drugs (actionability). (**B-D**) The percentage of cancer-associated LLPS scaffolds (**B**),
196 regulators (**C**) and clients (**D**) affected by various dominant mutation types is presented on the x axis, while their fold
197 enrichment values compared to COSMIC census as background is presented on the y axis. The truncating mutation
198 category comprises both frameshift and nonsense mutations.
199

200 To better understand their roles played in cancer development, we tested various features of cancer-
201 associated LLPS scaffolds, regulators and clients in comparison to all known cancer drivers from COSMIC
202 Census (**Table S6**). **Figure 4A** shows that LLPS scaffolds are enriched in oncogenes (see also **Figure S5**
203 where enrichment in oncogenes and tumor suppressors is confirmed based on comparisons against
204 equivalent randomized background sets) and are preferentially affected by dominant mutations (**Table**
205 **S7**). In contrast, LLPS regulators are slightly enriched in tumor suppressors and are targeted by dominant
206 mutations to a much lower degree. LLPS clients show no enrichment in either tumor suppressor/oncogene
207 role or in dominant/recessive mutations. This shows that on average the more significant role a protein

208 plays in phase separation (with scaffolds > regulators > clients), the more likely it is to be an oncogene
209 affected by dominant mutations.

210 Comparing the actionability – i.e. the number of FDA-approved drugs available – for various proteins, LLPS
211 scaffolds show an extreme depletion (**Figure 4A**). None of the 35 cancer-associated scaffolds have any
212 FDA-approved drugs, even considering off-label standard care use (*see Data and methods for definitions*).
213 LLPS regulators involved in tumorigenesis are also relatively poorly targetable, since only 2 out of the 36
214 proteins – KRAS and BRCA1 – have available drugs that act on them. In contrast, LLPS clients are generally
215 the most actionable with 22 out of 226 having available drugs (**Figure 4A** and **Table S7**).

216 Analyzing specific types of genetic alterations shows that all three classes of LLPS proteins are mostly
217 affected by the same three mutation types (**Figure 4B-D**): missense mutations (which have a local effect
218 on the protein); frameshift and nonsense mutations (which truncate the protein); and
219 translocations/fusions (which can create new proteins by combining regions of independent proteins into
220 a single product). Fusions/translocations were found to be the most abundant mutation type for LLPS
221 scaffolds. Although being only slightly enriched in this mutation type compared to cancer drivers in
222 general, 60% of the LLPS scaffolds form oncogenic fusions and for most of them this is the sole mutation
223 type observed in cancers (**Figure 4B**). In contrast, LLPS regulators are enriched in and are most often
224 affected by missense mutations, while LLPS clients show no enrichment in missense mutations and
225 fusions/translocations compared to cancer drivers in general. The tendencies proposed for LLPS scaffolds
226 are mostly confirmed by calculations made on PhaSepDB-derived scaffolds (**Figure S6**).
227

228 **5. Oncogenic fusion proteins represent novel combinations of functions driving tumorigenesis**
229

230 The analysis of COSMIC annotations clearly highlighted that LLPS scaffolds primarily contribute to cancer
231 through forming oncogenic fusion proteins (OFPs). Therefore, we performed a systematic analysis of the
232 known OFPs of COSMIC Census proteins. When assembling the OFP dataset, we deliberately followed a
233 highly selective approach in order to exclude passenger OFPs, which were just once observed in patient
234 samples through sequencing approaches and do not necessarily play a causal role in the respective cancer
235 type. For this reason we only used COSMIC-curated fusions and chose not to take OFPs from the TCGA
236 database (www.cancer.gov/tcga/), unlike the two recent studies analyzing the predicted LLPS propensities
237 of OFPs[50,51], who optimized on the abundance of data. Since the vast majority of the 32 TCGA cancer types
238 are typically not primarily relying on gene fusions/OFPs, while many rare cancer types are, we turned to
239 COSMIC, where rare cancer types often defined by the presence of a well-defined OFP (or a group of
240 those) are also covered, and only well-documented fusions of the Census proteins are listed that
241 recurrently occur in a particular cancer type and have a widely recognized role in driving oncogenesis. Of
242 the 450 unique fusion gene pairs identified for COSMIC Census genes, 303 in-frame-fused chimeric OFPs
243 could be obtained wherein each gene pair is represented by a single OFP and the fusion boundaries could
244 be precisely defined on the protein level (**Table S11**). Due to different data selection strategy and the
245 inclusion of rare cancer types, our 303 COSMIC-derived cancer driver OFPs only show a limited overlap
246 with the large sets of fusion oncoproteins recently analyzed for predicted LLPS propensities by Wang *et*

247 *al.*[51] and Tripathi *et al.*[50] (**Figure S7A**), therefore most of our annotated fusions remain unique to our
248 dataset and have never been investigated in relation to LLPS.
249
250 We analyzed our OFPs by scanning them for known conserved protein modules using Pfam, InterPro and
251 UniProt annotations (*see Data and methods and* **Tables S12-14**). Since the fusion breakpoints of well-
252 characterized OFPs tend to reside in disordered protein regions, leaving folded domains intact[53], we did
253 not have to deal with domains/modules cut into half by the fusions. Many protein modules perform
254 similar functions, therefore, we aimed at analyzing the molecular functions conveyed by them. These
255 functions can be captured using Gene Ontology (GO) terms, however, GO terms are assigned to full
256 proteins. To enable a systematic analysis of the associations between functions in the fusions, GO
257 molecular functions and biological processes were assigned to the protein modules of the collected OFPs
258 and their wild-type constituent proteins (**Figure 5A**; **Tables S15**-**S16**; see *Data and methods* for more
259 details). The GO terms assigned to the protein modules were mapped to a GO subset (GO Slim)
260 representing biologically relevant, fairly specific, yet high level processes and functions (**Table S17**).
261 Pairwise association levels were then determined for each possible pair of these processes/functions
262 assigned to the modules of the wild-type constituent proteins or OFPs, separately (see **Tables S18-S19** for
263 the resulting functional association matrices). The functions exhibiting significantly higher association
264 levels in OFPs were considered to be fusion-specific (**Figure 5A-B; Table S20**).
265

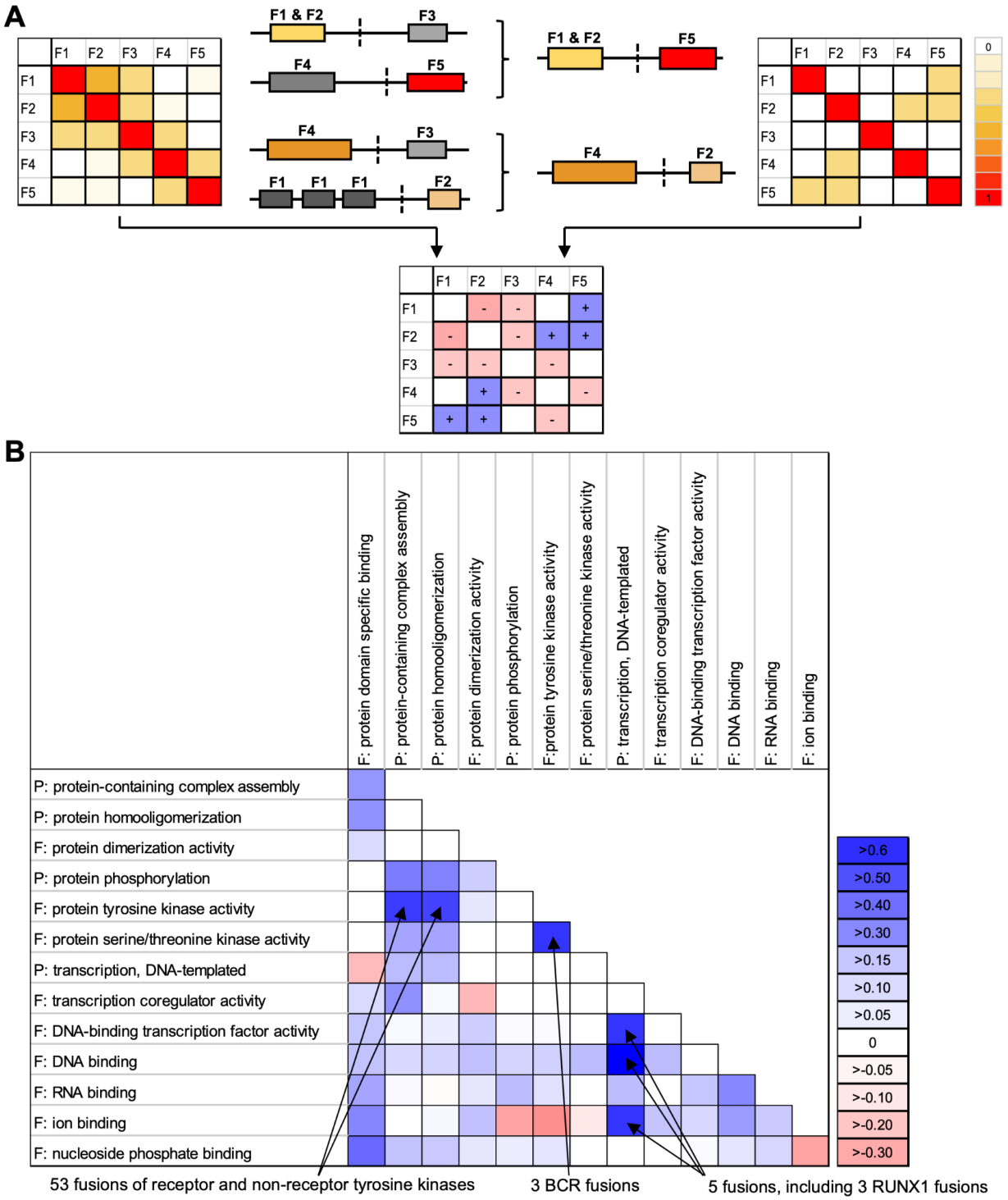


**Figure 5: Oncogenic fusion proteins represent novel combinations of molecular functions/processes.** (**A**) The functional modules of oncogenic fusion proteins (OFPs) and wild type constituent proteins were annotated by module-specific molecular functions/processes. Pairwise association levels between the annotated functions were calculated using overlap coefficients for OFPs and their constituent proteins separately. The association levels calculated for constituent proteins were subtracted from those calculated for OFPs to highlight the function pairs whose association levels are increased or decreased in OFPs. (**B**) Heatmap showing the pairwise associations

273 between functions (based on our GO Slim definition provided in **Table S17**) after removal of redundancy, for those
274 terms that are increased (shades of blue) or decreased (shades of red) in OFPs considerably (ΔOC ≥ 0.4 in **Table S20**).
275 Three additional terms are shown that do not fulfill the previous criterion but are important for our study and
276 generally considered to be linked to biomolecular condensation: protein phosphorylation, transcription coregulator
277 activity and RNA binding. The associations that showed the largest increase in OFPs (ΔOC > 0.5) are labeled with the
278 related fusion types. When calculating overlap coefficients, the number of elements in the intersection of the two
279 sets is divided by the size of the smaller set, therefore the resulting value will range from zero to one, irrespective
280 of the sizes of the two sets. Thus, it is possible for a set with only 3 BCR fusions to yield a comparable OC value as
281 over 50 RTK fusions.
282
283 Our data highlight strong fusion-specific association between tyrosine kinase activity (and the associated
284 protein phosphorylation function) and protein homooligomerization. Although the fusions of different
285 receptor tyrosine kinases (RTKs) are implicated in different cancer types, they all rely on very similar
286 molecular principles. In such fusions, RTKs lose their N-terminally encoded extracellular ligand-binding
287 domains and commonly their transmembrane segments too, while the fusion partners replacing those
288 can form homodimers or homo-oligomers. This leads to the dimerization, cross-phosphorylation and
289 constitutive activation of the tyrosine kinase domains and relocalization to the cytoplasm or nucleus
290 (depending on the partner). Consequently, this pathogenic process results in uncontrolled, ligand-
291 independent phosphorylation of their downstream target proteins[54,55]. Although this association has been
292 long recognized, to our knowledge, it has never been confirmed systematically on statistical terms. Our
293 dataset reveals over 50 OFPs showing an association of these two functions (an overlap coefficient (OC)
294 of 0.62 on a 0 - 1 scale for OFPs) while it does not occur in wild-type proteins (OC is 0.06; ΔOC=0.55)
295 (**Figure 5B, Tables S18, S19 and S20**). Breakpoint cluster region protein (BCR) fusions important in chronic
296 myeloid leukemia combine protein tyrosine kinase activity with protein serine-threonine kinase activity,
297 which does not exist in wild-type proteins (ΔOC=0.6). However, these fusions also represent a subset of
298 the fusions that combine oligomerization with tyrosine kinase activity. Oligomerization through BCR and
299 compromised regulation of the fused non-receptor tyrosine kinases lead to their over-activation, which is
300 central to oncogenicity (similarly to RTK fusions)[56–58]. Coupling of domains implicated in transcription
301 directly or as activators/repressors (covered by the term "transcription, DNA templated") with DNA-
302 binding domains (ΔOC=0.8 for "DNA-binding"), mainly zinc finger (ZnF) domains (ΔOC=0.6 for "ion-
303 binding") of transcription factors (ΔOC=0.6 for "DNA-binding transcription factor activity") is also specific
304 for certain fusions, e.g. a subset of RUNX1 fusions. In the OFPs of RUNX1/AML1 fused to members of the
305 CBFA2T family, the N-terminal DNA-binding RUNT domain of RUNX1 gets coupled to the TAFH, NHR2 and
306 MYND domains of CBFA2T family proteins, of which the TAFH domain is a protein-binding module involved
307 in transcription regulation[59]. A similar coupling is seen in the CBFA2T3-GLIS2 fusion where the TAFH
308 domain of CBFA2T3 gets coupled to the DNA-binding C2H2-type ZnF domains of GLIS2, and also in the
309 KMT2A-ELL fusion, where the DNA-binding CXXC-type ZnF of KMT2A gets coupled to ELL, which is part of
310 the transcription elongation factor complex, thus having a direct role in transcription. In all, our results
311 indicate that OFPs often exert their oncogenic effects through highly specific combinations of molecular
312 functions and that our data and approach are well-suited to detect those.
313

314 **6. Most oncogenic fusions of LLPS scaffolds couple phase separation with DNA-binding**

315

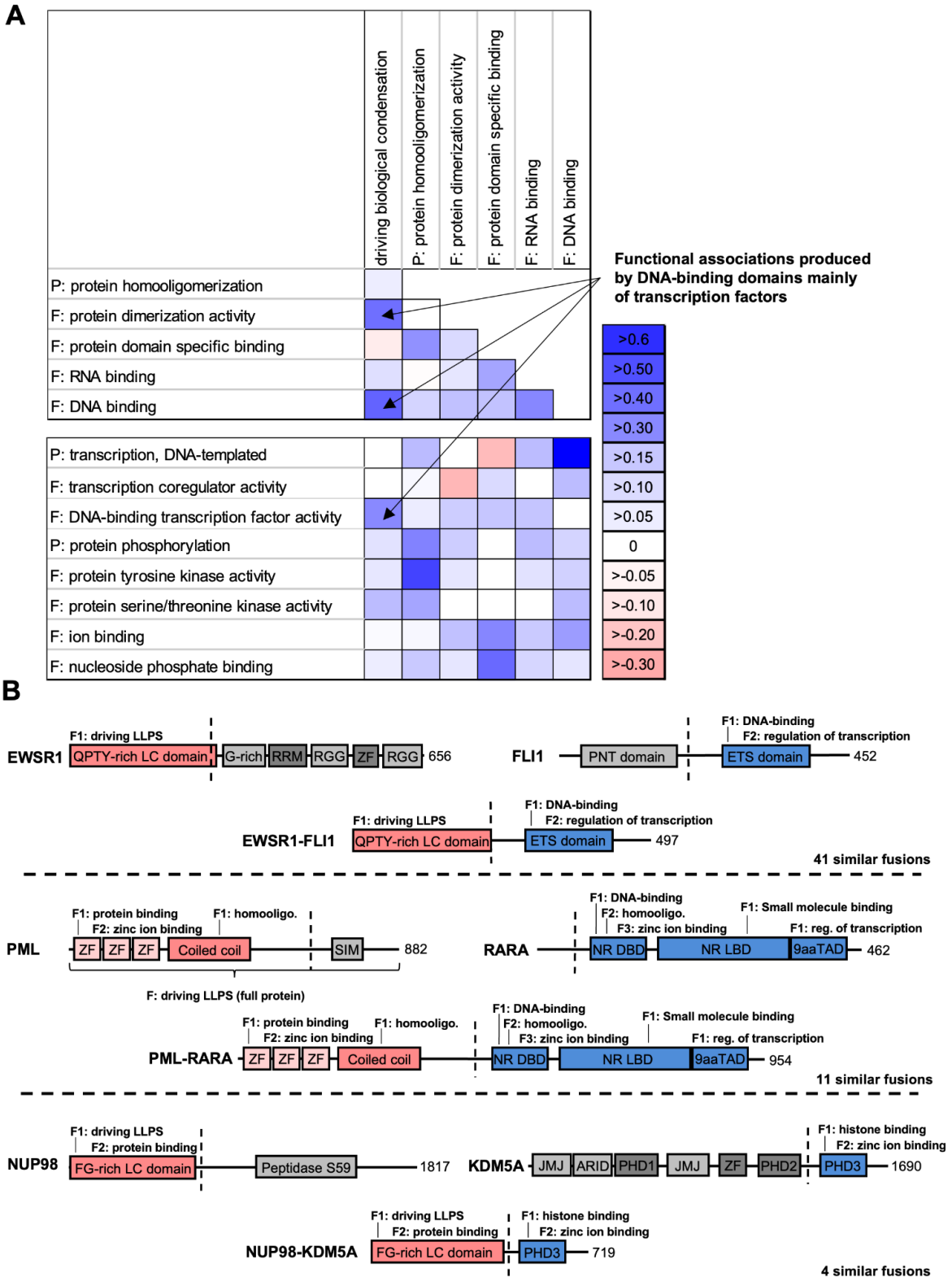


316

317

318 **Figure 6. Functional associations in the fusions of LLPS scaffolds.**
319 (**A**) The previous module-level functional annotations were complemented by assigning the function "driving
320 biomolecular condensation" to the regions of LLPS scaffolds that are minimally required for LLPS. Pairwise
321 association levels were calculated between "driving biomolecular condensation" and other molecular functions
322 important in condensate formation that capture the increase in valency or interaction capacity of the protein (see
323 symmetric heatmap on the top) as described in Figure 5, as well as between the condensate formation-associated
324 and the previously analyzed (Figure 5) molecular functions ('F') and biological processes ('P') (asymmetric heatmap
325 in the bottom). The heat maps show how pairwise associations between functions change in OFPs (shades of blue
326 for increase, shades of red for decrease). The functions associated with "driving biomolecular condensation" that
327 showed the largest increase in OFPs (ΔOC > 0.2) are labeled. (**B**) Domain maps and assigned module-level functions
328 of three well-studied, representative OFPs and their constituent proteins. Breakpoints of translocation are indicated
329 with vertical dashed lines. Assigned functions are only depicted for the protein modules that are retained in the
330 fusions, others are colored in shades of gray. Domains colored in red drive LLPS or homooligomerization, domains
331 colored in blue mediate transcription by DNA-binding or chromatin(histone)-binding. The different zinc fingers (ZFs)
332 of PML are colored light pink because they are not known to crucially contribute to the oncogenesis of the fusion
333 protein. The sizes of proteins and domains are not proportionate to each other. LC - low complexity, RRM - RNA-
334 recognition motif, ETS - erythroblast transformation specific domain, PNT - pointed domain, SIM - SUMO-interacting
335 motif, NR - nuclear receptor, DBD - DNA-binding domain, LBD - ligand-binding domain, TAD - transactivation domain,
336 PHD - plant homeodomain, JMJ - jumonji domain, homooligo. - homooligomerization, reg. - regulation.
337
338
339 Encouraged by the robust detection of function combinations already known to drive cancer, we
340 introduced "driving biomolecular condensation" as a novel molecular function term and assigned it to the
341 regions of LLPS scaffolds proposed to be minimally required for driving LLPS (**Table S21**). Then we
342 determined if the novel term shows any fusion-specific associations to other functions/processes as
343 described in the previous section (**Figure 6A**). Notably, most of the LLPS-driver regions of scaffolds are
344 largely retained in their fusions (in 69 of the 72 fusions), thus they were assigned with the "driving
345 biomolecular condensation" term. So, at least 69 fusions are expected to form condensates through LLPS
346 due to inheriting LLPS-driver regions. For 14 of these 69 fusions the ability to drive phase separation is
347 supported by two recent studies, where condensate localization of altogether 124 fusion oncoproteins
348 has been demonstrated in cells[50,51], while it was not disproved for any of them (**Figure S7B**). Interestingly,
349 LLPS scaffolds tend to be located on the N-terminus of the fusion products (in 63 of 72 cases; **Figure 6B**),
350 and since fusions always inherit the promoter and other gene regulatory regions of the N-terminally fused
351 gene, their expression will be mostly regulated by the gene regulatory regions of the LLPS scaffolds. These
352 LLPS-prone OFPs are typically implicated in early-onset soft tissue sarcomas and hematological
353 malignancies, while they are less involved in the development of the otherwise abundantly occurring brain
354 tumors, as well as late-onset carcinomas and skin cancers (**Figure 7**).
355

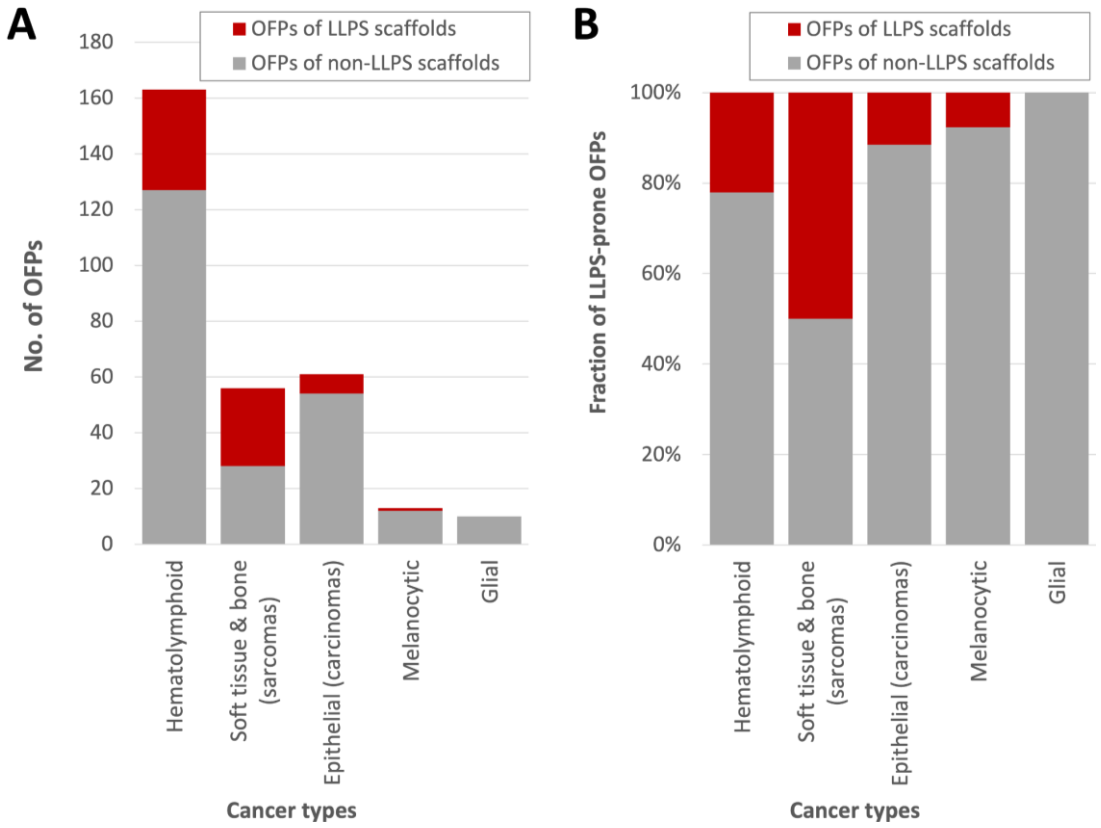


**Figure 7: The fraction of LLPS driver region-containing oncogenic fusion proteins (OFPs) in different categories of cancers.**

The absolute number (**panel A**) and relative percentage (**panel B**) of OFPs are shown in the five big categories of cancers defined by the developmental origin of the cancerous tissue. The OFPs that contain a known LLPS driver region are colored red, while those that do not are colored gray. For each OFP, the respective cancer type was obtained from the original data source (COSMIC/UniProt/original article). In the rare cases when more than one cancer type was indicated for the same OFP, the most frequently associated one was selected. Then these cancer types were grouped into five major categories defined by the developmental origin of the cancerous tissue (Supplementary Table S11). OFPs within the category of hematolymphoid cancers are implicated in lymphomas, leukemias and other neoplasms of myelocytes (e.g. myelodysplastic syndromes). OFPs of the soft tissue and bone category underlie the development of sarcomas but also some benign tumors of the soft tissues, such as lipomas. The OFPs observed in epithelial cancers (i.e. carcinomas) make up a distinct category. The category of melanocytic cancers involves OFPs implicated in skin tumors, such as melanomas and Spitz tumors. The category of glial cancers encompasses OFPs observed in malignancies of glial cells, including astrocytes.

The molecular function "driving biomolecular condensation" showed the strongest fusion-specific increase in association levels with the functions "DNA binding" (ΔOC=0.46), "protein dimerization activity" (ΔOC=0.42) and "DNA-binding transcription factor activity" (ΔOC=0.35) (**Figure 6A**). Other functions/processes did not exhibit strong (ΔOC>0.3) changes in associations. Association with "DNA binding" was found in 52 of the 69 LLPS-prone OFPs, a coupling of functions that has also been captured by Wang *et al.*[51]. Notably, "driving biomolecular condensation" and "DNA binding" are also moderately

379 associated in wild-type proteins (OC=0.38), probably because many transcription factors (TFs) have been
380 reported to phase-separate under certain conditions[60–62]. The other three detected functional
381 associations were somewhat weaker and were identified in subsets of the DNA-binding fusions – this is
382 not surprising, since a domain could have multiple annotated functions, and most DNA-binding domains
383 occur in TFs, many of which dimerize.
384
385 In 41 of the 52 fusions (all EWSR1, FUS and TAF15 fusions and 12 NUP98 fusions) that are typically
386 implicated in soft tissue sarcomas and hematological malignancies, respectively, a potent low-complexity
387 LLPS-prone region is coupled with an intact DNA-binding domain of certain transcription factors (mainly
388 ETS domain-containing TFs in FET fusions and homeobox TFs in NUP98 fusions) (**Figure 6B, Table S11**). In
389 the other 11 fusions with the same association, including PML-RARA, NPM1-RARA, BCOR-RARA, NUMA1-
390 RARA, STAT5B-RARA, ZBTB16-RARA, NPM1-MLF1, NONO-TFE3, SFPQ-TFE3, PAX5-ELN and PAX5-PML,
391 which are mainly associated with acute leukemias, an oligomerization-prone subregion of an LLPS-driver
392 or any other protein is combined with a TF (**Figure 6B**). (Since retinoic receptor alpha (RARα) is an LLPS
393 scaffold and it combines LLPS-prone disordered regions with a DNA-binding domain in itself[60], all its
394 fusions are a part of the dataset.) The LLPS propensity of the TFs is likely increased in their oligomerization-
395 prone fusions due to increased multivalency. At the same time, homo-oligomerization through an
396 extraneous domain can compromise certain functional modalities of the incorporated TFs (as seen for
397 PML-RARA[63,64] and NONO-TFE3[65]). Interestingly, these fusions not only differ from the fusions of the
398 previously introduced group based on the properties of the incorporated LLPS-prone regions, but they
399 also show different pathomechanisms. Most of them were shown to exert a dominant negative effect on
400 the transcriptional activity of the incorporated TFs that depends on the oligomerization of the fusion
401 partners[64,66–69]. Also, they may recruit activating and repressing chromatin remodeling complexes to
402 deregulate transcription[64,70].
403
404 Manual inspection of the domain structures of the 17 fusions that did not combine "driving biomolecular
405 condensation" with "DNA-binding" showed that 4 combine the LLPS-driver region of NUP98 with
406 chromatin-binding domains (displaying a similar pathomechanism to DNA binding NUP98 fusions[71])
407 (**Figure 6B**), 5 show associations between different oligomerization-prone subregions of LLPS scaffolds
408 and tyrosine kinase domains of RTKs (the molecular pathomechanism of these has been described in the
409 previous section), while the remaining 8 represent unique (e.g. DNAJB1-PRKACA[72]) or not completely clear
410 functional associations.
411

412 # Discussion

413
414 We set out to systematically study the connection between cancer and biological condensation,
415 specifically mapping the extent to which LLPS is affected in cancer and understanding the molecular
416 pathomechanisms and therapeutic consequences of mutations affecting LLPS scaffolds. Our motivation is
417 driven by our observation that out of diseases with a known causative protein repertoire, somatic cancer
418 has the strongest connection to LLPS scaffolds, far surpassing those of other diseases, including
419 neurodegenerative disorders where several such LLPS scaffolds are linked to disease emergence (**Figure**

420 **1**). In contrast, germline cancer mutations are extremely rare in LLPS scaffolds, indicating that these
421 mutations have a strong phenotypic effect, not tolerated to occur ubiquitously in the whole body. Our
422 high-level disease grouping demonstrates that there might be a correlation between disease severity and
423 involvement of LLPS, as many somatic cancers have much faster progression, if untreated, as compared
424 to cancer predisposition syndromes arising from germline cancer mutations or compared to
425 neurodegenerative diseases. This indicates that the modulation of LLPS scaffolds via cancer mutations
426 produces strong phenotypes. We focused on various aspects of tumorigenesis, ranging from mutational
427 mechanisms, through modulation of biological processes, up to the emergence of cellular hallmarks, to
428 understand why and how this happens.
429
430 Our data show that cancer-driving LLPS scaffolds are potent oncogenes, giving rise to dominant
431 phenotypes and lacking targeting options by current FDA-approved drugs (**Figure 4A**). These properties
432 not only contrast LLPS scaffolds with cancer drivers in general, but also with cancer drivers playing a
433 regulator or client role in LLPS. Therefore, the mutation or dysregulation of proteins directly involved in
434 inducing biological condensation gives rise to the most detrimental phenotypes. Many studies have
435 provided insights into these genetic alterations showing that overexpression or missense mutations can
436 produce gain or loss of function for LLPS scaffolds[25,43–48]. However, we found that 60% of the cancer-
437 driving LLPS scaffolds are predominantly affected by gene fusions that create oncogenic fusion proteins
438 (OFPs) (**Figure 4B**). This is in agreement with individual cases where LLPS scaffolds were found to
439 contribute to different cancer types through forming OFPs[48,73]. OFPs display diverse pathomechanisms[74],
440 they could alter the regulation or localization of important hub proteins thereby rewiring protein
441 interaction networks[75–77], and/or introduce specific combinations of protein domains/functions that have
442 a high potential for driving cancer[47,53,54]. In a high-throughput study, a large set of TCGA-derived OFPs
443 (with yet-unvalidated roles in the respective cancer types) were analyzed for various LLPS-associated
444 predicted features and 166 were tested for punctate/condensate localization in HeLa cells[50]. This study
445 concluded that the majority of fusion oncoproteins are likely to partition into condensates, and
446 highlighted important physicochemical features associated with nuclear and cytoplasmic condensation.
447 Furthermore, they derived 4 major archetypical classes of OFPs, and using the set of computed features
448 developed a prediction tool to analyze the LLPS-propensity of OFPs in high throughput[50].
449
450 Importantly, several OFPs of LLPS scaffolds have been already shown to undergo LLPS, such as those of
451 the FET family proteins (FUS, EWSR1 and TAF15)[78–82] and nucleoporins[73,83–85], and some others, such as
452 NONO-TFE3[65], SS18-SSX[86], BRD4-NUTM1[87], SFPQ-TFE3[51]. Most of these fusion products are primary
453 drivers of cancer (primarily of sarcomas and hematolymphoid cancers, as shown in **Figure 7**), i.e. they are
454 potent oncogenes with the ability to drive the tumorigenic transformation of healthy cells by
455 themselves[64,88–92]. In their case, oncogenicity is mostly attributed to their ability to form condensates at
456 non-native subcellular locations[48].
457
458 The mechanism of action of OFPs fundamentally differs from other cancer-mutated proteins[74], as they
459 can combine molecular functions in a novel way that is detrimental to the healthy cell, driving oncogenic
460 transformation[53], as exemplified by RTK fusions[25,54,76]. We explored this functional association by attaching
461 functional annotations to protein regions that can be identified in any protein sequence in an automated

462 and high-throughput way (**Figure 5**). Through systematic analysis, we found that the vast majority of OFPs
463 that contain regions of LLPS scaffolds inherit the ability to drive phase separation, and we propose that
464 they can be classified into 4 main categories: low complexity LLPS scaffolds coupled with DNA-binding via
465 1) transcription factor (TF) domains or 2) chromatin-binding domains; and oligomerization-prone
466 subregions of LLPS scaffolds fused to 3) TFs or 4) receptor tyrosine kinase domains (**Figure 6**). Category 1
467 is specific for soft tissue sarcomas (FET family fusions) or acute leukemias (NUP98 fusions), categories 2
468 and 3 are mainly responsible for acute leukemias, and category 4) shows no obvious cancer type
469 specificity. Nonetheless, fusions of the first three categories all seem to rely on similar molecular
470 principles, representing potent, LLPS-prone transcriptional activators[78] or repressors[93].
471
472 A likely reason for the strong detrimental phenotypic effect of LLPS-scaffold OFPs belonging to the first
473 three categories is that the combination of TF activity with the ability to self-sufficiently initiate phase
474 separation is uncommon in a healthy cell. Wild-type TFs tested for LLPS so far could only phase-separate
475 on their own at high concentrations[60,61], which is in conflict with their otherwise notoriously low cellular
476 levels[7]. At near-physiological concentrations, TFs require at least a coactivator and a specific DNA segment
477 for LLPS[62], therefore, they are typically context- and partner-dependent LLPS scaffolds. In contrast, in the
478 context of fusions TFs are complemented by potent LLPS-driver regions or at least by homo-
479 oligomerization domains and display elevated expression levels due to the exchange of their gene
480 regulatory regions, which both favor condensate formation. Therefore, such fusions resolve the
481 dependencies of the incorporated TFs and form ectopic condensates along the DNA even at genes which
482 are not normally regulated by the TF[69,94,95]. Such condensates act as potent transcriptional activators or
483 repressors by efficiently recruiting diverse chromatin remodeling complexes[64,69–71,96–101] (or even RNA
484 polymerase II itself[78,102]), leading to aberrant gene expression patterns[34,103]. The pathomechanisms of
485 many fusions in our dataset (see **Figure 6B** for examples and **Table S11** for a full list of fusion constructs)
486 have been studied individually, however, our results underscore that they represent a much larger group
487 of LLPS-prone OFPs that combine similar functions and thus likely rely on similar underlying molecular
488 principles.
489
490 This unique molecular makeup of LLPS-scaffold OFPs is reflected in the biological processes the cancer-
491 associated LLPS scaffolds are involved in. By performing enrichment analysis using standard Gene
492 Ontology (GO) terms, we can recapitulate that the most affected processes are chromatin remodeling, as
493 well as mRNA-related terms (**Figure 3**). For instance, the nucleolar protein nucleophosmin is a regulator
494 of mRNA splicing that functions in chromatin remodeling[104–106], however, it often forms oncogenic fusions
495 resulting in loss of function in lymphomas[107]. In contrast, regulators of LLPS implicated in cancer are
496 responsible for gene expression-related processes, as well as controlling the creation, breakdown and
497 localization of proteins (**Figure 3**). While these processes are often modulated in cancer in general, LLPS-
498 related proteins play a disproportionately large role in their modulation. The unique nature of cancer-
499 associated LLPS scaffolds becomes even more evident when moving to a higher level. By defining toolkits
500 and supertoolkits, i.e. higher and higher level aggregates of GO terms, it becomes clear that LLPS scaffolds
501 are primarily centered on the maintenance and organization of the genetic material and the regulation of
502 protein availability, as opposed to response to stimuli and the flow of information inside the cell, which
503 are most characteristic of cancer drivers in general (**Figure 3**). At a higher functional level, all these cancer-

504 related processes translate into cellular phenotypes, often referred to as the ten hallmarks of cancer[52]. In
505 this regard, the observed aggressive tumorigenic property can be attributed to the fact that all hallmarks
506 of cancer can emerge from the mutation of LLPS scaffolds, and most hallmarks are significantly enriched
507 in these proteins (**Figure 2**). Furthermore, cancer-driving LLPS scaffolds are often multifunctional proteins
508 in the hallmark space, thus their mutations can contribute to several hallmarks at once, driving
509 tumorigenesis and cancer progression more efficiently.
510
511 The aggressive dominant cellular effect of fusions created by LLPS scaffolds is further exacerbated by the
512 fact that the resulting OFPs tend to be modular, large and largely disordered[53], meaning that finding a
513 single compound to inhibit them is likely to be challenging. In reality, none of the cancer-driving LLPS
514 scaffolds in our dataset has any FDA-approved drug (**Figure 4A**), in line with previous studies of LLPS-prone
515 OFPs[64]. When targeting LLPS-prone proteins or OFPs, many factors need to be considered, for instance,
516 that the partitioning, concentration and activity of cancer drugs may be influenced by the physicochemical
517 attributes of the MLOs[108]. Despite these difficulties, there are a few drugs under development that could
518 target a limited set of LLPS-prone fusion proteins, such as the BRD4-NUTM fusion in midline carcinoma[87]
519 or LLPS scaffolds fused to RTKs or other kinases potentially being amenable for treatment with kinase
520 inhibitors[55,72,107]. Recently, Wang *et al.* set up a high-throughput imaging-based assay (DropScan) to
521 reassess anticancer drugs as condensate inhibitors, and managed to identify a handful of compounds of
522 low target-specificity that efficiently dissolved condensates of transcriptional OFPs, further validating the
523 direct condensate modulation approach[51]. Furthermore, the pathogenic effects of certain LLPS-prone
524 fusions could potentially be targeted indirectly, through modulating, for instance, their crucial interaction
525 partners, transcriptional targets or the activity of certain chromatin remodeling complexes[64,85,109,110].
526
527 Finding novel strategies for targeting LLPS-inducing OFPs is not just a matter of combating a few obscure
528 cancer cases. While our current analysis only encompasses 69 such fusions due to the limited number of
529 experimentally validated LLPS scaffolds, the true number of OFPs with LLPS scaffolding properties is likely
530 to be much higher, as also suggested by Tripathi *et al.*[50]. We observed a general increase in associations
531 between LLPS-related functions that increase the valency and the interaction capacity of the generated
532 OFPs, such as oligomerization, protein domain specific binding, RNA binding and DNA binding (**Figure 6A**
533 upper matrix). Also, through predictions, we found that OFPs in general display a very high propensity for
534 LLPS, way higher than cancer drivers in general, and strikingly, on par with experimentally validated LLPS
535 scaffolds (**Figure 8**). This is likely due to cases where the individual constituent proteins of the fusion
536 construct cannot induce phase separation, but the fusion protein can, such as the EML4-ALK and CCDC6-
537 RET fusions[76,111,112]. In this light, finding the currently missing drugs to shut down OFPs[64], to disrupt the
538 condensation enabled by them[51,113], and to offset their downstream effects[64,85,109] could provide cancer
539 drugs widely applicable to diverse cancer incidences previously defying standard treatments.
540

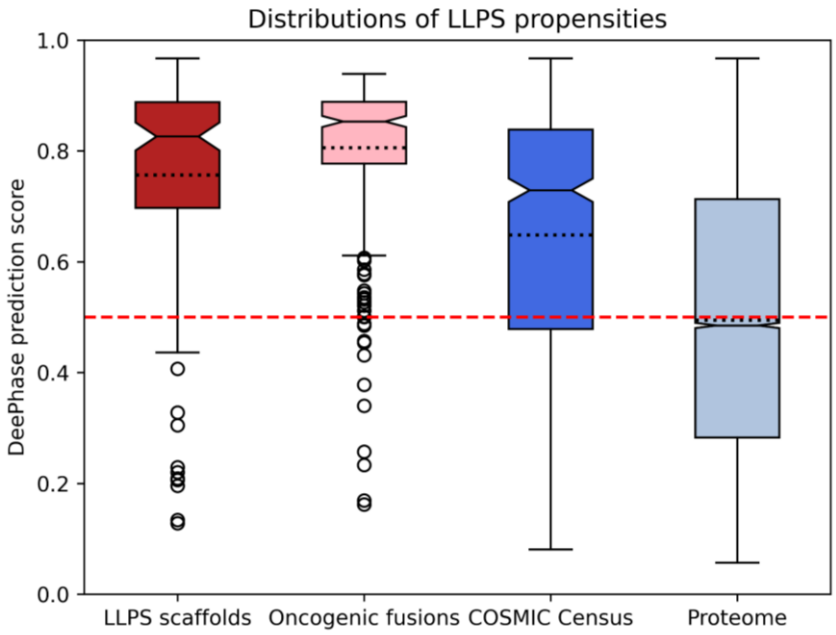


**Figure 8: Distributions of predicted LLPS propensities for four different protein groups.** LLPS propensity was predicted by DeepPhase for 4 groups of proteins: LLPS scaffolds (red), oncogenic fusion proteins (pink), cancer drivers from COSMIC Census (dark blue) and the whole human proteome (light blue). The continuous horizontal line on the boxes shows the median, while the dotted line indicates the mean of the distribution. The red dashed line is drawn at 0.5, the cutoff value for LLPS on the DeePhase score.

# Data and methods

## 1. Assembly of datasets

### *1.1. LLPS-related proteins*

LLPS scaffold proteins were taken as the consolidated dataset of 87 proteins from[7], and were extended with 54 manually curated proteins totalling 141 high-confidence human LLPS scaffolds. 344 human LLPS regulators were derived from DrLLPS[19] and 3,503 clients from various data resources (PhaSepDB v1.3[20], DrLLPS[19], MSGP[114], RNP granule DB[115], MiCroKiTS[116]) that provide information on the localizations of proteins to MLOs (see **Table S1**). Additionally, another larger set of less confident LLPS scaffolds (containing a certain number of clients that have been demonstrated to partition into already existing condensates in *in vitro* experiments) were retrieved from a newer version of PhaSepDB (version 2.1)[117] presenting a dataset of 859 proteins from low throughput experiments. The obtained proteins were filtered for unique human proteins and the resulting set of 271 proteins (**Table S4**) (which contains 56 COSMIC Census proteins) was used as an independent alternative of our high-confidence scaffold dataset.

565 ***1.2. Cancer drivers from the COSMIC Census and their actionability from OncoKB***
566 Somatic cancer driver proteins were taken from the Census of COSMIC v95 (**Table S6**). Both tier 1 and tier
567 2 proteins were used, together with annotations of dominant mutation types, involvement in cancer
568 hallmarks, and molecular roles. Actionability data was taken from OncoKB[118]. Only proteins with an
569 actionability level 1 or 2, i.e. proteins for which there exists at least one FDA-approved drug (level 1), or a
570 drug that is used as standard care (level 2) were considered actionable in our analyses.
571
572 ***1.3. Germline cancer-related proteins***
573 Germline cancer-related genes with mutations in protein coding regions were obtained from ClinVar[119]
574 and HUMSAVAR (https://www.uniprot.org/docs/humsavar) (both downloaded in September 2021) and
575 limited to records with the cancer-related disease terms available in **Supplementary data file 1**. ClinVar
576 classifies phenotype-genotype relationships into groups ranging from less reliable to definite links. To
577 achieve high confidence, entries with "limited", "disputed", "no known disease relationship", "refuted"
578 relationships were not accepted. HUMSAVAR genotype-phenotype records were filtered for the ones
579 accompanied by OMIM phenotype identifiers. The resulting dataset of proteins is available as **Table S2**.
580
581 ***1.4. Neurodegenerative disease-linked proteins***
582 ClinVar[119] and HUMSAVAR (https://www.uniprot.org/docs/humsavar) were downloaded in September
583 2021, and genes that have neurodegenerative disease-linked mutations in protein coding regions were
584 selected. To achieve this, the dataset was filtered for a curated list of expressions related to
585 neurodegenerative diseases – the precise search terms are available in **Supplementary data file 1**, while
586 the resulting dataset is available as **Table S2**. Entries with the four least confident phenotype-genotype
587 relationship categories were excluded again, as explained previously in *Data and methods section 1.3*.
588 Finally, the remaining mutations that did not match either germline cancer- or neurodegenerative
589 disease-associated terms were included into the "other hereditary diseases" category.
590
591 ***1.5. Amyloid fiber-forming proteins***
592 Human amyloid fiber-forming proteins were retrieved from the AmyPro database[120] in August 2021 (**Table**
593 **S5**).
594
595 ***1.6 Subcellular localization for the full human proteome***
596 We defined the subcellular localization for each protein in the human proteome by integrating data from
597 Gene Ontology annotations in UniProt (GOA), UniProt annotations, the Human Transmembrane
598 Proteome (HTP)[121], MatrixDB[122], and MatrisomeDB[123]. We divided the UniProt and the Gene Ontology
599 annotations (GOA) into tier 1 (more reliable) and tier 2 (less reliable) annotations, depending on the
600 attached evidence codes. For UniProt, annotations with the evidence codes ECO:0000269 or ECO:0000305
601 are considered as tier 1, while annotations with evidence codes ECO:0000250, ECO:0000255, or
602 ECO:0000303 are tier 2. For Gene Ontology, annotations with evidence codes IDA, IMP, IPI, IGI, EXP, IBA,
603 IKR, TAS, NAS, IC, or ND are tier 1, while annotations with evidence codes HDA, ISS, ISA, RCA, ISO, ISM,
604 IGC, or IEA are tier 2.
605 Based on these, each protein was assigned exactly one broad localization. It was considered to be a
606 transmembrane protein (TMP), if it is assigned the 'integral component of membrane (GO:0016021)' GO

term in tier 1 GOA annotations, or it is annotated as a TMP in HTP with a confidence score over 85, or is annotated in HTP as a TMP with a confidence score above 50 and is also annotated as a TMP in GOA (either tier). TMPs were further categorized into *Plasmamembrane TMPs* (if they had the 'plasma membrane (GO:0005886)' GO annotation in either tier of GOA, or had any of the following terms in their tier 1 or tier 2 UniProt annotations: cell membrane, postsynaptic density membrane, flagellum membrane, cilium membrane, dendritic spine membrane, filopodium membrane, growth cone membrane, invadopodium membrane, lamellipodium membrane, microvillus membrane, podosome membrane, pseudopodium membrane, ruffle membrane, stereocilium membrane), *Internal membrane TMPs* (if annotated with any of the intracellular localizations, see below), *External membrane TMPs* (if annotated with any of the extracellular localizations, see below), and *TMPs in unknown membrane* (if none of the previous categories could be assigned).

Proteins (TMP and non-TMP) were annotated with the following intracellular localizations:

- nuclear, if it has the 'nucleus (GO:0005634)' term attached in GOA tier 1, or the 'Nucleus' term attached in UniProt tier 1; or if it has no tier 1 annotations, but is attached the same GO term in GOA tier 2, or the same UniProt term in tier 2;
- cytosol, if it has the 'cytosol (GO:0005829)' term attached in GOA tier 1, or the 'Cytosol' term attached in UniProt tier 1; or if it has no tier 1 annotations, but is attached the same GO term in GOA tier 2, or the same UniProt term in tier 2;
- nucleus/cytoplasm shuttling, if it can be annotated both as a nuclear and a cytosolic protein based on the above definitions;
- ER, if it has the 'endoplasmic reticulum (GO:0005783)' term attached in GOA tier 1, or any of the 'Endoplasmic reticulum', 'Endoplasmic reticulum lumen' and 'Endoplasmic reticulum membrane' terms attached in UniProt tier 1; or if it has no tier 1 annotations, but is attached the same GO term in GOA tier 2, or the same UniProt term in tier 2;
- Golgi, if it has the 'Golgi apparatus (GO:0005794)' term attached in GOA tier 1, or if it has no tier 1 annotations, but is attached the same GO term in GOA tier 2, or the 'Golgi apparatus' annotation in UniProt tier 2;
- cytoskeleton, if it has the 'cytoskeleton (GO:0005856)' term attached in GOA tier 1, or the 'cytoskeleton' term attached in UniProt tier 1; or if it has no tier 1 annotations, but is attached the same GO term in GOA tier 2, or the same UniProt term in tier 2;
- mitochondrium, if it has the 'mitochondrion (GO:0005739)' term attached in GOA tier 1, or the 'Mitochondrion' term attached in UniProt tier 1; or if it has no tier 1 annotations, but is attached the same GO term in GOA tier 2, or the same UniProt term in tier 2;
- other intracellular organelle, if it has the 'intracellular anatomical structure (GO:0005622)' term attached in GOA tier 1, or the 'Cytoplasm' term attached in UniProt tier 1, and cannot be assigned any of the above, more specific localizations; or if it has no tier 1 annotations, but is attached the same GO term in GOA tier 2, or the same UniProt term in tier 2.

Or if none of these could be assigned, then one of the following extracellular localizations:

- extracellular vesicle, if it has any of the 'exosome (GO:0070062)', 'microvesicle (GO:1990742)', or 'prominosome (GO:0071914)' terms attached in GOA tier 1, or either the 'extracellular vesicle' or 'extracellular exosome' term attached in UniProt tier 1; or if it has no tier 1 annotations, but is attached the same GO term in GOA tier 2, or the same UniProt term in tier 2;

649 ● extracellular, if it has any of the 'extracellular space (GO:0005615)', 'collagen trimer
650 (GO:0005581)' or 'complex of collagen trimers (GO:0098644)' terms attached in GOA tier 1, or the
651 'Mitochondrion' term attached in UniProt tier 1; or if it has no tier 1 annotations, but is attached
652 the same GO term in GOA tier 2, or the same UniProt term in tier 2.
653 If none of these terms could be defined for the protein, it was classified as 'Unknown localization'.
654 The list of subcellular localizations for all human proteins is shown in **Table S3**.
655
656
657 ***1.7. Randomized selections of human proteins from UniProt to gain unbiased background sets for***
658 ***statistical comparisons***
659
660 Cancer-associated proteins in the COSMIC Census are usually highly researched owing to their established
661 disease link. Thus, these proteins usually have high annotation scores in UniProt with many Gene Ontology
662 (GO) terms associated with them. In addition, cancer-associated proteins are often plasmamembrane
663 receptors and transcription factors, leading to a non-uniform distribution across various subcellular
664 localizations. These deviations from the average human proteins would lead to severe annotation biases
665 in our enrichment calculations. Therefore, in each such analysis, we compare the COSMIC Census proteins
666 to random sets of proteins that share the same annotation score in UniProt (5 out of 5) and the same
667 distribution across various subcellular localizations (as defined above). We generated 1000 sets of
668 randomly selected proteins from the human proteome that have the same number of proteins, all with a
669 UniProt annotation score of 5, and the same subcellular localization distribution as the set of proteins we
670 are assessing, for instance, COSMIC Census proteins. This procedure was applied to gain unbiased
671 randomized background sets for all disease protein sets, separately (see **Supplementary data files 2-5**),
672 as well as for oncogenes and tumor suppressors (**Supplementary data files 6-7**).
673
674 ***1.8. Oncogenic fusions***
675
676 ***1.8.1. Assembling data on the oncogenic fusion proteins of all COSMIC Census proteins***
677
678 We performed a comprehensive, protein-level manual curation of the OFPs of all COSMIC Census proteins,
679 where fusion was provided as a dominant mutation type. For these proteins, each of their fusion partners
680 listed either by COSMIC or UniProt were collected, and the corresponding fusion gene pairs annotated,
681 totaling 450 unique gene pairs.
682
683 Fusions of the same two genes that only differ in their fusion breakpoints were considered as variants of
684 the same fusion and not as distinct fusions, so only one representative was annotated. Only in-frame
685 fusions of two different genes were considered, where the resulting fusion protein contained in-frame
686 portions of any size of both encoded proteins, including those cases where a short non-coding (usually
687 intronic) segment separates two in-frame protein-coding regions. For the fusion gene pairs for which at
688 least one COSMIC sample and fusion identifier was available, we selected the most frequently occurring
689 fusion setup/breakpoint (the one indicated with the most samples) and made an attempt to annotate the
690 exact protein boundaries based on that. A preference was given to fusion identifiers/transcript-level

691 descriptions, wherein the transcript boundaries were well-defined (lacking +/- and ? characters marking
692 lack of confidence in fusion boundaries). The UniProt isoforms corresponding to the indicated Ensemble
693 transcript identifiers could be unambiguously identified in each case. For the N-terminal fusion partner
694 we obtained the protein boundary by taking the indicated fusion breakpoint of the transcript, subtracting
695 the length of the 5'UTR and dividing the remaining number (length of CDS before the breakpoint) by 3.
696 The integer portion of the result was accepted as the protein level fusion breakpoint for the N-terminal
697 gene. If the remainder after dividing by 3 was not zero, we made a note of that to see if the fusion is in-
698 frame or not. For the transcript of the C-terminal gene, based on the first nucleotide indicated by COSMIC
699 to be part of the fusion, we calculated the length of the CDS that was missing from the fusion and divided
700 it by 3 to see how many residues were missing from the N-terminus of the protein. The remainder (if any)
701 was compared to the previously noted remainder of the N-terminal gene. If the two remainders were
702 equal, that means that the N-terminal portion of the first gene could substitute for the N-terminal portion
703 of the second gene in a way that the reading frame was preserved, so the fusion was accepted to be an
704 in-frame fusion.
705
706 The fused regions' boundaries were annotated in a way that only residues entirely encoded by the
707 respective coding regions have been accepted. De novo residues made up by the fused codons or
708 originally non-coding spacer regions were not added to any of the two protein regions, but were noted as
709 middle residues (if they could be identified). In the majority of the cases, where the fusions were
710 annotated based on COSMIC fusion transcripts, the middle residues could not be identified, only the
711 number of nucleotides the two different genes contributed to the encoding of the middle residue. We
712 noted this as 2+1 or 1+2, where the contribution of the N-terminal gene is the first number and the
713 contribution of the C-terminal gene is the second number.
714
715 For the fusion partners, where the fusion breakpoints were not provided by COSMIC or UniProt, those
716 were obtained through comprehensive literature curation of the associated articles. In these cases, we
717 revisited the original articles where the precise boundary of the fusion was described (usually the first
718 article reporting on the fusion of the two genes).
719
720 The integrated table with the resulting manually curated oncogenic fusions from UniProt and COSMIC is
721 available as **Table S11**. In the table it is also provided if at least one of the fusion partners of the OFPs is
722 an LLPS driver, so those could be separately analyzed.
723
724 **2. Assembly of the molecular toolkits**
725 Inspired by an earlier cancer analysis paper[124], we created a large compilation of 21 molecular toolkits
726 belonging to 5 higher level categories ('supertoolkits'), defined based on GO annotations available for
727 proteins[125,126]. These encompass a diverse set of functions that cover a broad range of actions proteins
728 carry out within human tissues comprising amongst others genome organization, regulation of protein
729 availability, transport-related, signaling-related and other processes (**Figure 3A**).
730 Description of the toolkit and supertoolkit definitions along with the exact GO terms defining the given
731 molecular toolkits are listed in **Tables S8 and S9**.

732 Toolkit enrichment for LLPS categories (scaffold, regulator, client) was compared to the presence of toolkit
733 terms in cancer drivers, while the enrichment of toolkits for cancer drivers was contrasted with an
734 equivalent, unbiased, randomized background (**Supplementary data file 2**). Both were quantified by fold
735 enrichment values and the p-values of Fisher's exact tests (**Table S10**).
736
737
738 **3. Domain mapping, functional annotation of domains and enrichment analysis**
739
740 ***3.1. Identifying InterPro, Pfam, and UniProt regions***
741 Pfam[127] (downloaded on February 24, 2023) and InterPro[128] (version 5.56) annotations were used to scan
742 both cancer driver proteins, as well as OFPs. UniProt region annotations were taken from the UniProt
743 database, downloaded on October 7, 2022. UniProt regions were assigned to OFPs if the fusion construct
744 contained at least 10% of the residues in the original region. While this cutoff is low, for structured regions
745 (such as domains, DNA-binding regions, etc), it is virtually always the case that the fusion product either
746 contains all of the region or none of it[53]. Fractions of UniProt regions only show up in fusion constructs
747 where the region denotes a region without well-defined tertiary structure or if the region is repetitive in
748 nature, such as coiled coils. In these cases, the permissive 10% cutoff ensures that we capture functionality
749 arising from only a portion of the region.
750
751 ***3.2. Gene Ontology annotations of Pfam, InterPro, and UniProt regions***
752 Identified InterPro and Pfam regions were attached with Gene Ontology (GO) terms using various sources
753 (**Tables S12 and S13**). The InterPro2GO and Pfam2GO mappings were downloaded from the EBI servers
754 on June 20, 2022. In addition, we further annotated various Pfam regions based on literature sources:
755 RNA binding function (GO:0003723) was assigned to Pfam domains and families in the EuRBPDB[129], while
756 DNA binding function (GO:0003677) based on prior efforts of Malhotra & Sowdhamini[130], and
757 phospholipid binding (GO:0005543) based on MBPpred[131]. Protein dimerization (GO:0046983),
758 homooligomerization (GO:0051260) and complex oligomerization (GO:0051259) were annotated based
759 on relevant articles[132] and additional manual curation efforts. Chromatin modifiers were stringently re-
760 curated starting from an earlier study[133], and domains were functionally mapped to a small set of GO
761 terms with varying annotation depth related to chromatin modification.
762
763 For UniProt regions/domains/sites/motifs annotated to more than one oncogenic fusions, these protein
764 components were functionally characterized by GO terms using manual curation (**Table S14**). Additionally,
765 some of the UniProt regions occurring only once in the protein set were also functionally annotated. In
766 total more than 800 GO terms were manually assigned to these UniProt regions from a set of 27 GO-
767 defined molecular functions or biological processes. One of the most common UniProt regions in our set
768 was the term "coiled-coil region" (126 occurrences), for which functional annotation is less trivial. For
769 simplicity, the GO term "protein homooligomerization" (GO:0051260) was assigned to it as a proxy.
770 InterPro and Pfam domains listed in the ELM database[134] (downloaded on September 28, 2022) as binding
771 partners for any motif were annotated with the 'GO:0019904, protein domain specific binding' term.

The InterPro/Pfam/UniProt - GO associations were then used to attach GO annotations to cancer proteins (**Table S15**) and OFPs (**Table S16**). These GO terms were then mapped to a GO subset (GO Slim) that represents biologically relevant, fairly specific yet high level processes and functions (**Table S17**).

### *3.3 Mapping the minimal regions of LLPS scaffolds and labeling them by annotations*

The minimal LLPS regions of the fusion-forming LLPS scaffolds were derived from *in vitro* experiments describing the minimal requirements of LLPS in the references provided in **Table S21**. Annotation of the term "driving biological condensation" to (fusion) proteins followed similar rules as for UniProt annotations. This label was considered together with the GO terms and is also shown in **Tables S15-20**.

### *3.4. Enrichment analysis of functional region associations*

We analyzed how commonly pairs of functional categories (defined by GO terms) of different protein domains and regions associate to each other in cancer proteins in general, and also in oncogenic fusion proteins in specific (**Tables S18-19**). Functional term associations were defined by the overlap coefficient metric (also known as Szymkiewicz–Simpson coefficient): $OC(X,Y) = |X \cap Y| / \min(|X|,|Y|)$.
Enrichment of associations was defined as a simple difference of overlap coefficients ($\Delta OC = OC1 - OC2$). **Table S20** shows the differences of these overlap coefficients between the cancer proteins and OFPs.

## 4. Large-scale prediction of LLPS propensity

DeePhase[135], Droppler[136], PSPredictor[137] and GraPES[138] were benchmarked on our LLPS scaffold set. GraPES predictions were accessed from the online database, and the MaGS Z-scores were converted using the (z+1)/3 formula and capped at [0,1]. The rest of the predictors gave numbers within [0,1]. While DeePhase and PSPredictor are parameter-free and only take the sequence as input, Doppler had to be run by setting the experimental conditions for which we chose the default parameters (T=37°C, c=10uM, pH=7, I=0.01M, crowder=None).
The LLPS propensity scores for each protein were compiled as distributions for each predictor, and evaluated as quartiles and upper/lower interquartile ranges * 1.5 (IQR*1.5) visualized as box-whisker plots (python 3.10; using package 'matplotlib' version 2.6.3). DeePhase was selected for proteome-wide LLPS propensity prediction as its propensity distribution including the data points ranging from the upper to the lower whisker were best overlapping with the 0.5-1.0 normalized LLPS propensity range, while other predictors more often predicted lower LLPS propensities (<0.5) for experimentally validated LLPS scaffolds. Proteome-wide LLPS propensity prediction (**Table S22**) was performed on the UniProt-assembled human reference proteome (UP000005640) downloaded in May 2022 (**Table S3**). From this dataset two selections were made: a subset for the LLPS scaffolds and a subset for the cancer drivers from COSMIC Census (**Supplementary data file 8**). Lastly, LLPS propensities were also predicted (**Table S23**) by DeePhase for reconstituted sequences of oncogenic fusion proteins (*see Data and methods subsection 1.8* and **Supplementary data file 9**).

### 5. Statistical analyses

χ2 statistics were applied to address the statistical significance of overlaps between LLPS scaffolds and various disease-associated proteins using the reviewed human proteome (20,359 proteins) from UniProt as a background. Generally human LLPS proteins are very well annotated, in comparison to many non-LLPS proteins. Therefore, to obtain a proper baseline devoid of any bias resulting from retrieving random proteins from human proteome which are either understudied or belonging to a subcellular localization irrelevant to LLPS, for example extracellular proteins, we filter the whole human proteome to proteins that are similarly well annotated and distributed within the cell. Subsequently, the obtained subset was used as a background for performing the random selections of proteins to serve as reference sets for the significance tests.

Due to the smaller data sizes, we chose to apply Fisher's exact test using the 713 COSMIC cancer genes as background in statistical analyses of the association between LLPS and cancer hallmarks or other characteristics including molecular toolkits. In the case of molecular toolkits, the overrepresentation of cancer drivers among the proteins of the human proteome belonging to each toolkit was evaluated by comparisons to a background consisting of 100 randomized datasets with an equivalent number of proteins. The overrepresentation values of cancer drivers served as a baseline to evaluate the extent and significance of toolkit enrichments of the cancer-associated proteins of the 3 LLPS groups.

# Acknowledgements and funding

This project has been implemented with the support provided by the Ministry of Innovation and Technology of Hungary from the National Research, Development and Innovation Fund, financed under the K-124670 and K-131702 funding schemes granted to P.T. and the FK-128133 and FK-142285 funding schemes granted to R.P. R.P is a holder of the János Bolyai Research Fellowship of the Hungarian Academy of Sciences (BO/00174/22). This work was supported by an EC H2020-WIDESPREAD-2020-5 Twinning grant 'PhasAge' (no. 952334 to P.T.). N.F is a PhD fellow supported by an FWO fellowship in fundamental research (FWOTM1124). T.L. is a postdoctoral innovation mandate holder (HBC.2022.0194) of the Flanders Innovation & Entrepreneurship Agency (VLAIO). B.M. thanks ALSAC for funding and support for his research.

# Conflict of interest

The authors declare that they do not have a conflict of interest.

850 # References


851 1. Shin, Y. & Brangwynne, C. P. Liquid phase condensation in cell physiology and disease. *Science* **357**,
852 (2017).
853 2. Brangwynne, C. P. *et al.* Germline P granules are liquid droplets that localize by controlled
854 dissolution/condensation. *Science* **324**, 1729–1732 (2009).
855 3. Alberti, S., Gladfelter, A. & Mittag, T. Considerations and Challenges in Studying Liquid-Liquid Phase
856 Separation and Biomolecular Condensates. *Cell* **176**, 419–434 (2019).
857 4. Pancsa, R., Schad, E., Tantos, A. & Tompa, P. Emergent functions of proteins in non-stoichiometric
858 supramolecular assemblies. *Biochim. Biophys. Acta: Proteins Proteomics* (2019)
859 doi:10.1016/j.bbapap.2019.02.007.
860 5. Mészáros, B. *et al.* PhaSePro: the database of proteins driving liquid-liquid phase separation.
861 *Nucleic Acids Res.* **48**, D360–D367 (2020).
862 6. Banani, S. F., Lee, H. O., Hyman, A. A. & Rosen, M. K. Biomolecular condensates: organizers of
863 cellular biochemistry. *Nat. Rev. Mol. Cell Biol.* **18**, 285–298 (2017).
864 7. Farahi, N., Lazar, T., Wodak, S. J., Tompa, P. & Pancsa, R. Integration of Data from Liquid-Liquid
865 Phase Separation Databases Highlights Concentration and Dosage Sensitivity of LLPS Drivers. *Int. J.*
866 *Mol. Sci.* **22**, (2021).
867 8. Das, S., Lin, Y.-H., Vernon, R. M., Forman-Kay, J. D. & Chan, H. S. Comparative roles of charge, , and
868 hydrophobic interactions in sequence-dependent phase separation of intrinsically disordered
869 proteins. *Proc. Natl. Acad. Sci. U. S. A.* **117**, 28795–28805 (2020).
870 9. Vernon, R. M. *et al.* Pi-Pi contacts are an overlooked protein feature relevant to phase separation.
871 *Elife* **7**, (2018).
872 10. Wang, J. *et al.* A Molecular Grammar Governing the Driving Forces for Phase Separation of Prion-
873 like RNA Binding Proteins. *Cell* **174**, 688–699.e16 (2018).

874 11. Van Roey, K. *et al.* Short linear motifs: ubiquitous and functionally diverse protein interaction
875 modules directing cell regulation. *Chem. Rev.* **114**, 6733–6778 (2014).
876 12. Su, X. *et al.* Phase separation of signaling molecules promotes T cell receptor signal transduction.
877 *Science* **352**, 595–599 (2016).
878 13. Li, P. *et al.* Phase transitions in the assembly of multivalent signalling proteins. *Nature* **483**, 336–340
879 (2012).
880 14. Boeynaems, S. *et al.* Protein Phase Separation: A New Phase in Cell Biology. *Trends in Cell Biology*
881 vol. 28 420–435 Preprint at https://doi.org/10.1016/j.tcb.2018.02.004 (2018).
882 15. Roden, C. & Gladfelter, A. S. RNA contributions to the form and function of biomolecular
883 condensates. *Nat. Rev. Mol. Cell Biol.* (2020) doi:10.1038/s41580-020-0264-6.
884 16. Van Lindt, J. *et al.* F/YGG-motif is an intrinsically disordered nucleic-acid binding motif. *RNA Biol.* **19**,
885 622–635 (2022).
886 17. Mitrea, D. M. *et al.* Methods for Physical Characterization of Phase-Separated Bodies and
887 Membrane-less Organelles. *J. Mol. Biol.* **430**, 4773–4805 (2018).
888 18. Li, Q. *et al.* LLPSDB: a database of proteins undergoing liquid-liquid phase separation in vitro.
889 *Nucleic Acids Res.* **48**, D320–D327 (2020).
890 19. Ning, W. *et al.* DrLLPS: a data resource of liquid-liquid phase separation in eukaryotes. *Nucleic Acids*
891 *Res.* **48**, D288–D295 (2020).
892 20. You, K. *et al.* PhaSepDB: a database of liquid-liquid phase separation related proteins. *Nucleic Acids*
893 *Res.* **48**, D354–D359 (2020).
894 21. Pancsa, R., Vranken, W. & Mészáros, B. Computational resources for identifying and describing
895 proteins driving liquid-liquid phase separation. *Brief. Bioinform.* (2021) doi:10.1093/bib/bbaa408.
896 22. Guo, Y. E. *et al.* Pol II phosphorylation regulates a switch between transcriptional and splicing
897 condensates. *Nature* **572**, 543–548 (2019).

898 23. Sabari, B. R. *et al.* Coactivator condensation at super-enhancers links phase separation and gene
899 control. *Science* **361**, (2018).
900 24. Hnisz, D., Shrinivas, K., Young, R. A., Chakraborty, A. K. & Sharp, P. A. A Phase Separation Model for
901 Transcriptional Control. *Cell* **169**, 13–23 (2017).
902 25. Mehta, S. & Zhang, J. Liquid-liquid phase separation drives cellular function and dysfunction in
903 cancer. *Nat. Rev. Cancer* (2022) doi:10.1038/s41568-022-00444-7.
904 26. Alberti, S. & Dormann, D. Liquid-Liquid Phase Separation in Disease. *Annu. Rev. Genet.* **53**, 171–194
905 (2019).
906 27. Zhang, L. *et al.* Phase-Separated Subcellular Compartmentation and Related Human Diseases. *Int. J.*
907 *Mol. Sci.* **23**, (2022).
908 28. Babinchak, W. M. & Surewicz, W. K. Liquid-Liquid Phase Separation and Its Mechanistic Role in
909 Pathological Protein Aggregation. *J. Mol. Biol.* **432**, 1910–1925 (2020).
910 29. Zbinden, A., Pérez-Berlanga, M., De Rossi, P. & Polymenidou, M. Phase Separation and
911 Neurodegenerative Diseases: A Disturbance in the Force. *Dev. Cell* **55**, 45–68 (2020).
912 30. Patel, A. *et al.* A Liquid-to-Solid Phase Transition of the ALS Protein FUS Accelerated by Disease
913 Mutation. *Cell* **162**, 1066–1077 (2015).
914 31. Alberti, S. & Hyman, A. A. Biomolecular condensates at the nexus of cellular stress, protein
915 aggregation disease and ageing. *Nat. Rev. Mol. Cell Biol.* **22**, 196–213 (2021).
916 32. Boyko, S. & Surewicz, W. K. Tau liquid-liquid phase separation in neurodegenerative diseases.
917 *Trends Cell Biol.* **32**, 611–623 (2022).
918 33. Calabretta, S. & Richard, S. Emerging Roles of Disordered Sequences in RNA-Binding Proteins.
919 *Trends Biochem. Sci.* **40**, 662–672 (2015).
920 34. Cai, D., Liu, Z. & Lippincott-Schwartz, J. Biomolecular Condensates and Their Links to Cancer
921 Progression. *Trends Biochem. Sci.* **46**, 535–549 (2021).

922 35. Bouchard, J. J. *et al.* Cancer Mutations of the Tumor Suppressor SPOP Disrupt the Formation of
923 Active, Phase-Separated Compartments. *Mol. Cell* **72**, 19–36.e8 (2018).
924 36. Zhu, G. *et al.* Phase Separation of Disease-Associated SHP2 Mutants Underlies MAPK
925 Hyperactivation. *Cell* **183**, 490–502.e18 (2020).
926 37. Raymond-Smiedy, P., Bucknor, B., Yang, Y., Zheng, T. & Castañeda, C. A. A Spectrophotometric
927 Turbidity Assay to Study Liquid-Liquid Phase Separation of UBQLN2 In Vitro. *Methods Mol. Biol.*
928 **2551**, 515–541 (2023).
929 38. Song, L. *et al.* Hotspot mutations in the structured ENL YEATS domain link aberrant transcriptional
930 condensates and cancer. *Mol. Cell* **82**, 4080–4098.e12 (2022).
931 39. Meng, F. *et al.* Induced phase separation of mutant NF2 imprisons the cGAS-STING machinery to
932 abrogate antitumor immunity. *Mol. Cell* **81**, 4147–4164.e7 (2021).
933 40. Shi, B. *et al.* UTX condensation underlies its tumour-suppressive activity. *Nature* **597**, 726–731
934 (2021).
935 41. Tsang, B., Pritišanac, I., Scherer, S. W., Moses, A. M. & Forman-Kay, J. D. Phase Separation as a
936 Missing Mechanism for Interpretation of Disease Mutations. *Cell* **183**, 1742–1756 (2020).
937 42. Banani, S. F. *et al.* Genetic variation associated with condensate dysregulation in disease. *Dev. Cell*
938 **57**, 1776–1788.e8 (2022).
939 43. Nozawa, R.-S. *et al.* Nuclear microenvironment in cancer: Control through liquid-liquid phase
940 separation. *Cancer Sci.* **111**, 3155–3163 (2020).
941 44. Boija, A., Klein, I. A. & Young, R. A. Biomolecular Condensates and Cancer. *Cancer Cell* **39**, 174–192
942 (2021).
943 45. Jiang, S., Fagman, J. B., Chen, C., Alberti, S. & Liu, B. Protein phase separation and its role in
944 tumorigenesis. *Elife* **9**, (2020).
945 46. Taniue, K. & Akimitsu, N. Aberrant phase separation and cancer. *FEBS J.* **289**, 17–39 (2022).

946 47. Quiroga, I. Y., Ahn, J. H., Wang, G. G. & Phanstiel, D. Oncogenic fusion proteins and their role in
947 three-dimensional chromatin structure, phase separation, and cancer. *Curr. Opin. Genet. Dev.* **74**,
948 101901 (2022).
949 48. Davis, R. B., Moosa, M. M. & Banerjee, P. R. Ectopic biomolecular phase transitions: fusion proteins
950 in cancer pathologies. *Trends Cell Biol.* **32**, 681–695 (2022).
951 49. Shirnekhi, H. K., Chandra, B. & Kriwacki, R. W. The role of phase-separated condensates in fusion
952 oncoprotein–driven cancers. *Annu. Rev. Cancer Biol.* **7**, (2023).
953 50. Tripathi, S. *et al.* Defining the condensate landscape of fusion oncoproteins. *Nat. Commun.* **14**,
954 6008 (2023).
955 51. Wang, Y. *et al.* Dissolution of oncofusion transcription factor condensates for cancer therapy. *Nat.*
956 *Chem. Biol.* **19**, 1223–1234 (2023).
957 52. Hanahan, D. & Weinberg, R. A. Hallmarks of cancer: the next generation. *Cell* **144**, 646–674 (2011).
958 53. Hegyi, H., Buday, L. & Tompa, P. Intrinsic structural disorder confers cellular viability on oncogenic
959 fusion proteins. *PLoS Comput. Biol.* **5**, e1000552 (2009).
960 54. Nelson, K. N., Peiris, M. N., Meyer, A. N., Siari, A. & Donoghue, D. J. Receptor Tyrosine Kinases:
961 Translocation Partners in Hematopoietic Disorders. *Trends Mol. Med.* **23**, 59–79 (2017).
962 55. Vaishnavi, A., Le, A. T. & Doebele, R. C. TRKing down an old oncogene in a new era of targeted
963 therapy. *Cancer Discov.* **5**, 25–34 (2015).
964 56. Ren, R. Mechanisms of BCR-ABL in the pathogenesis of chronic myelogenous leukaemia. *Nat. Rev.*
965 *Cancer* **5**, 172–183 (2005).
966 57. Hantschel, O. & Superti-Furga, G. Regulation of the c-Abl and Bcr-Abl tyrosine kinases. *Nat. Rev.*
967 *Mol. Cell Biol.* **5**, 33–44 (2004).
968 58. Woessner, D. W. *et al.* A coiled-coil mimetic intercepts BCR-ABL1 dimerization in native and kinase-
969 mutant chronic myeloid leukemia. *Leukemia* **29**, 1668–1675 (2015).

970 59. Wei, Y. *et al.* A TAF4-homology domain from the corepressor ETO is a docking platform for positive
971 and negative regulators of transcription. *Nat. Struct. Mol. Biol.* **14**, 653–661 (2007).
972 60. Boija, A. *et al.* Transcription Factors Activate Genes through the Phase-Separation Capacity of Their
973 Activation Domains. *Cell* **175**, 1842–1855.e16 (2018).
974 61. Nair, S. J. *et al.* Phase separation of ligand-activated enhancers licenses cooperative chromosomal
975 enhancer assembly. *Nat. Struct. Mol. Biol.* **26**, 193–203 (2019).
976 62. Shrinivas, K. *et al.* Enhancer Features that Drive Formation of Transcriptional Condensates. *Mol. Cell*
977 **75**, 549–561.e7 (2019).
978 63. Perez, A. *et al.* PMLRAR homodimers: distinct DNA binding properties and heteromeric interactions
979 with RXR. *EMBO J.* **12**, 3171–3182 (1993).
980 64. Brien, G. L., Stegmaier, K. & Armstrong, S. A. Targeting chromatin complexes in fusion protein-
981 driven malignancies. *Nat. Rev. Cancer* **19**, 255–269 (2019).
982 65. Wang, B. *et al.* The positive regulation loop between NRF1 and NONO-TFE3 fusion promotes phase
983 separation and aggregation of NONO-TFE3 in NONO-TFE3 tRCC. *Int. J. Biol. Macromol.* **176**, 437–
984 447 (2021).
985 66. Weterman, M. A., van Groningen, J. J., Tertoolen, L. & van Kessel, A. G. Impairment of MAD2B-PRCC
986 interaction in mitotic checkpoint defective t(X;1)-positive renal cell carcinomas. *Proc. Natl. Acad.*
987 *Sci. U. S. A.* **98**, 13808–13813 (2001).
988 67. Kurahashi, S. *et al.* PAX5-PML acts as a dual dominant-negative form of both PAX5 and PML.
989 *Oncogene* **30**, 1822–1830 (2011).
990 68. Bousquet, M. *et al.* A novel PAX5-ELN fusion protein identified in B-cell acute lymphoblastic
991 leukemia acts as a dominant negative on wild-type PAX5. *Blood* **109**, 3417–3423 (2007).
992 69. De Braekeleer, E., Douet-Guilbert, N. & De Braekeleer, M. RARA fusion genes in acute
993 promyelocytic leukemia: a review. *Expert Rev. Hematol.* **7**, 347–357 (2014).

994 70. Darracq, A. *et al.* NPM and NPM-MLF1 interact with chromatin remodeling complexes and
995 influence their recruitment to specific genes. *PLoS Genet.* **15**, e1008463 (2019).
996 71. Xu, H. *et al.* NUP98 Fusion Proteins Interact with the NSL and MLL1 Complexes to Drive
997 Leukemogenesis. *Cancer Cell* **30**, 863–878 (2016).
998 72. Zhang, J. Z. *et al.* Phase Separation of a PKA Regulatory Subunit Controls cAMP Compartmentation
999 and Oncogenic Signaling. *Cell* **182**, 1531–1544.e15 (2020).
1000 73. Ahn, J. H. *et al.* Phase separation drives aberrant chromatin looping and cancer development.
1001 *Nature* **595**, 591–595 (2021).
1002 74. Latysheva, N. S. & Babu, M. M. Discovering and understanding oncogenic gene fusions through data
1003 intensive computational approaches. *Nucleic Acids Res.* **44**, 4487–4503 (2016).
1004 75. Latysheva, N. S. *et al.* Molecular Principles of Gene Fusion Mediated Rewiring of Protein Interaction
1005 Networks in Cancer. *Mol. Cell* **63**, 579–592 (2016).
1006 76. Tulpule, A. *et al.* Kinase-mediated RAS signaling via membraneless cytoplasmic protein granules.
1007 *Cell* **184**, 2649–2664.e18 (2021).
1008 77. Terlecki-Zaniewicz, S. *et al.* Biomolecular condensation of NUP98 fusion proteins drives
1009 leukemogenic gene expression. *Nat. Struct. Mol. Biol.* **28**, 190–201 (2021).
1010 78. Kwon, I. *et al.* Phosphorylation-regulated binding of RNA polymerase II to fibrous polymers of low-
1011 complexity domains. *Cell* **155**, 1049–1060 (2013).
1012 79. Davis, R. B., Kaur, T., Moosa, M. M. & Banerjee, P. R. FUS oncofusion protein condensates recruit
1013 mSWI/SNF chromatin remodeler via heterotypic interactions between prion-like domains. *Protein*
1014 *Sci.* **30**, 1454–1466 (2021).
1015 80. Owen, I. *et al.* The oncogenic transcription factor FUS-CHOP can undergo nuclear liquid-liquid phase
1016 separation. *J. Cell Sci.* **134**, (2021).
1017 81. Zuo, L. *et al.* Loci-specific phase separation of FET fusion oncoproteins promotes gene transcription.

1018 *Nat. Commun.* **12**, 1491 (2021).

1019 82. Chong, S. *et al.* Tuning levels of low-complexity domain interactions to modulate endogenous
1020 oncogenic transcription. *Mol. Cell* **82**, 2084–2097.e5 (2022).

1021 83. Chandra, B. *et al.* Phase Separation Mediates NUP98 Fusion Oncoprotein Leukemic Transformation.
1022 *Cancer Discov.* **12**, 1152–1169 (2022).

1023 84. Port, S. A. *et al.* The Oncogenic Fusion Proteins SET-Nup214 and Sequestosome-1 (SQSTM1)-
1024 Nup214 Form Dynamic Nuclear Bodies and Differentially Affect Nuclear Protein and Poly(A)+ RNA
1025 Export. *J. Biol. Chem.* **291**, 23068–23083 (2016).

1026 85. Mendes, A., Jühlen, R., Martinelli, V. & Fahrenkrog, B. Targeted CRM1-inhibition perturbs
1027 leukemogenic NUP214 fusion proteins and exerts anti-cancer effects in leukemia cell lines with
1028 rearrangements. *Oncotarget* **11**, 3371–3386 (2020).

1029 86. Cheng, Y. *et al.* Phase transition and remodeling complex assembly are important for SS18-SSX
1030 oncogenic activity in synovial sarcomas. *Nat. Commun.* **13**, 2724 (2022).

1031 87. Rosencrance, C. D. *et al.* Chromatin Hyperacetylation Impacts Chromosome Folding by Forming a
1032 Nuclear Subcompartment. *Mol. Cell* **78**, 112–126.e12 (2020).

1033 88. Kroon, E., Thorsteinsdottir, U., Mayotte, N., Nakamura, T. & Sauvageau, G. NUP98-HOXA9
1034 expression in hemopoietic stem cells induces chronic and acute myeloid leukemias in mice. *EMBO J.*
1035 **20**, 350–361 (2001).

1036 89. Lin, Y.-W., Slape, C., Zhang, Z. & Aplan, P. D. NUP98-HOXD13 transgenic mice develop a highly
1037 penetrant, severe myelodysplastic syndrome that progresses to acute leukemia. *Blood* **106**, 287–
1038 295 (2005).

1039 90. Westervelt, P. *et al.* High-penetrance mouse model of acute promyelocytic leukemia with very low
1040 levels of PML-RARalpha expression. *Blood* **102**, 1857–1865 (2003).

1041 91. Riggi, N. *et al.* EWS-FLI-1 expression triggers a Ewing's sarcoma initiation program in primary human

1042 mesenchymal stem cells. *Cancer Res.* **68**, 2176–2185 (2008).

1043 92. Haldar, M., Hancock, J. D., Coffin, C. M., Lessnick, S. L. & Capecchi, M. R. A conditional mouse model
1044 of synovial sarcoma: insights into a myogenic origin. *Cancer Cell* **11**, 375–388 (2007).

1045 93. Yamamoto, Y. *et al.* BCOR as a novel fusion partner of retinoic acid receptor alpha in a
1046 t(X;17)(p11;q12) variant of acute promyelocytic leukemia. *Blood* **116**, 4274–4283 (2010).

1047 94. Gangwal, K. *et al.* Microsatellites as EWS/FLI response elements in Ewing's sarcoma. *Proc. Natl.*
1048 *Acad. Sci. U. S. A.* **105**, 10149–10154 (2008).

1049 95. Rio-Machin, A. *et al.* The molecular pathogenesis of the NUP98-HOXA9 fusion protein in acute
1050 myeloid leukemia. *Leukemia* **31**, 2000–2005 (2017).

1051 96. Kasper, L. H. *et al.* CREB binding protein interacts with nucleoporin-specific FG repeats that activate
1052 transcription and mediate NUP98-HOXA9 oncogenicity. *Mol. Cell. Biol.* **19**, 764–776 (1999).

1053 97. Valerio, D. G. *et al.* Histone Acetyltransferase Activity of MOF Is Required for Leukemogenesis.
1054 *Cancer Res.* **77**, 1753–1762 (2017).

1055 98. Shima, Y., Yumoto, M., Katsumoto, T. & Kitabayashi, I. MLL is essential for NUP98-HOXA9-induced
1056 leukemia. *Leukemia* **31**, 2200–2210 (2017).

1057 99. Franks, T. M. *et al.* Nup98 recruits the Wdr82-Set1A/COMPASS complex to promoters to regulate
1058 H3K4 trimethylation in hematopoietic progenitor cells. *Genes Dev.* **31**, 2222–2234 (2017).

1059 100. Riggi, N. *et al.* EWS-FLI1 utilizes divergent chromatin remodeling mechanisms to directly activate or
1060 repress enhancer elements in Ewing sarcoma. *Cancer Cell* **26**, 668–681 (2014).

1061 101. Boulay, G. *et al.* Cancer-Specific Retargeting of BAF Complexes by a Prion-like Domain. *Cell* **171**,
1062 163–178.e19 (2017).

1063 102. Wei, M.-T. *et al.* Nucleated transcriptional condensates amplify gene expression. *Nat. Cell Biol.* **22**,
1064 1187–1196 (2020).

1065 103. Wang, G. G., Cai, L., Pasillas, M. P. & Kamps, M. P. NUP98-NSD1 links H3K36 methylation to Hox-A

1066 gene activation and leukaemogenesis. *Nat. Cell Biol.* **9**, 804–812 (2007).
1067 104. Tarapore, P. *et al.* Thr199 phosphorylation targets nucleophosmin to nuclear speckles and
1068 represses pre-mRNA processing. *FEBS Lett.* **580**, 399–409 (2006).
1069 105. Okuwaki, M. *et al.* Function of homo- and hetero-oligomers of human
1070 nucleoplasmin/nucleophosmin family proteins NPM1, NPM2 and NPM3 during sperm chromatin
1071 remodeling. *Nucleic Acids Res.* **40**, 4861–4878 (2012).
1072 106. Ugolini, I. *et al.* Chromatin localization of nucleophosmin organizes ribosome biogenesis. *Mol. Cell*
1073 **82**, 4443–4457.e9 (2022).
1074 107. Werner, M. T., Zhao, C., Zhang, Q. & Wasik, M. A. Nucleophosmin-anaplastic lymphoma kinase: the
1075 ultimate oncogene and therapeutic target. *Blood* **129**, 823–831 (2017).
1076 108. Klein, I. A. *et al.* Partitioning of cancer therapeutics in nuclear condensates. *Science* **368**, 1386–1392
1077 (2020).
1078 109. Schmoellerl, J. *et al.* CDK6 is an essential direct target of NUP98 fusion proteins in acute myeloid
1079 leukemia. *Blood* **136**, 387–400 (2020).
1080 110. Oka, M. *et al.* Chromatin-prebound Crm1 recruits Nup98-HoxA9 fusion to induce aberrant
1081 expression of Hox cluster genes. *Elife* **5**, e09540 (2016).
1082 111. Qin, Z. *et al.* Phase separation of EML4-ALK in firing downstream signaling and promoting lung
1083 tumorigenesis. *Cell Discov* **7**, 33 (2021).
1084 112. Sampson, J., Richards, M. W., Choi, J., Fry, A. M. & Bayliss, R. Phase-separated foci of EML4-ALK
1085 facilitate signalling and depend upon an active kinase conformation. *EMBO Rep.* **22**, e53693 (2021).
1086 113. Mitrea, D. M., Mittasch, M., Gomes, B. F., Klein, I. A. & Murcko, M. A. Modulating biomolecular
1087 condensates: a novel approach to drug discovery. *Nat. Rev. Drug Discov.* **21**, 841–862 (2022).
1088 114. Nunes, C. *et al.* MSGP: the first database of the protein components of the mammalian stress
1089 granules. *Database* **2019**, (2019).

1090 115. Millar, S. R. *et al.* A New Phase of Networking: The Molecular Composition and Regulatory
1091 Dynamics of Mammalian Stress Granules. *Chem. Rev.* **123**, 9036–9064 (2023).
1092 116. Huang, Z. *et al.* MiCroKiTS 4.0: a database of midbody, centrosome, kinetochore, telomere and
1093 spindle. *Nucleic Acids Res.* **43**, D328–34 (2015).
1094 117. Hou, C. *et al.* PhaSepDB in 2022: annotating phase separation-related proteins with droplet states,
1095 co-phase separation partners and other experimental information. *Nucleic Acids Res.* **51**, D460–
1096 D465 (2023).
1097 118. Chakravarty, D. *et al.* OncoKB: A Precision Oncology Knowledge Base. *JCO Precis Oncol* **2017**,
1098 (2017).
1099 119. Landrum, M. J. *et al.* ClinVar: improving access to variant interpretations and supporting evidence.
1100 *Nucleic Acids Res.* **46**, D1062–D1067 (2018).
1101 120. Varadi, M., De Baets, G., Vranken, W. F., Tompa, P. & Pancsa, R. AmyPro: a database of proteins
1102 with validated amyloidogenic regions. *Nucleic Acids Res.* **46**, D387–D392 (2018).
1103 121. Dobson, L., Reményi, I. & Tusnády, G. E. The human transmembrane proteome. *Biol. Direct* **10**, 31
1104 (2015).
1105 122. Clerc, O. *et al.* MatrixDB: integration of new data with a focus on glycosaminoglycan interactions.
1106 *Nucleic Acids Res.* **47**, D376–D381 (2019).
1107 123. Shao, X., Taha, I. N., Clauser, K. R., Gao, Y. T. & Naba, A. MatrisomeDB: the ECM-protein knowledge
1108 database. *Nucleic Acids Res.* **48**, D1136–D1144 (2020).
1109 124. Mészáros, B., Hajdu-Soltész, B., Zeke, A. & Dosztányi, Z. Mutations of Intrinsically Disordered
1110 Protein Regions Can Drive Cancer but Lack Therapeutic Strategies. *Biomolecules* **11**, (2021).
1111 125. Ashburner, M. *et al.* Gene ontology: tool for the unification of biology. The Gene Ontology
1112 Consortium. *Nat. Genet.* **25**, 25–29 (2000).
1113 126. Gene Ontology Consortium. The Gene Ontology resource: enriching a GOld mine. *Nucleic Acids Res.*

1114 **49**, D325–D334 (2021).

1115 127. Mistry, J. *et al.* Pfam: The protein families database in 2021. *Nucleic Acids Res.* **49**, D412–D419
1116 (2021).

1117 128. Paysan-Lafosse, T. *et al.* InterPro in 2022. *Nucleic Acids Res.* **51**, D418–D427 (2023).

1118 129. Liao, J.-Y. *et al.* EuRBPDB: a comprehensive resource for annotation, functional and oncological
1119 investigation of eukaryotic RNA binding proteins (RBPs). *Nucleic Acids Res.* **48**, D307–D313 (2020).

1120 130. Malhotra, S. & Sowdhamini, R. Collation and analyses of DNA-binding protein domain families from
1121 sequence and structural databanks. *Mol. Biosyst.* **11**, 1110–1118 (2015).

1122 131. Nastou, K. C., Tsaousis, G. N., Papandreou, N. C. & Hamodrakas, S. J. MBPpred: Proteome-wide
1123 detection of membrane lipid-binding proteins using profile Hidden Markov Models. *Biochim.*
1124 *Biophys. Acta* **1864**, 747–754 (2016).

1125 132. Uguzzoni, G. *et al.* Large-scale identification of coevolution signals across homo-oligomeric protein
1126 interfaces by direct coupling analysis. *Proc. Natl. Acad. Sci. U. S. A.* **114**, E2662–E2671 (2017).

1127 133. Pu, S. *et al.* Expanding the landscape of chromatin modification (CM)-related functional domains
1128 and genes in human. *PLoS One* **5**, e14122 (2010).

1129 134. Kumar, M. *et al.* The Eukaryotic Linear Motif resource: 2022 release. *Nucleic Acids Res.* **50**, D497–
1130 D508 (2022).

1131 135. Saar, K. L. *et al.* Learning the molecular grammar of protein condensates from sequence
1132 determinants and embeddings. *Proc. Natl. Acad. Sci. U. S. A.* **118**, (2021).

1133 136. Raimondi, D. *et al.* In-silico prediction of in-vitro protein liquid-liquid phase separation experiments
1134 outcomes with multi-head neural attention. *Bioinformatics* (2021)
1135 doi:10.1093/bioinformatics/btab350.

1136 137. Chu, X. *et al.* Prediction of liquid-liquid phase separating proteins using machine learning. *BMC*
1137 *Bioinformatics* **23**, 72 (2022).

1138 138. Kuechler, E. R., Jacobson, M., Mayor, T. & Gsponer, J. GraPES: The Granule Protein Enrichment
1139 Server for prediction of biological condensate constituents. *Nucleic Acids Res.* **50**, W384–91 (2022).

1140